

**Infrared Colors and Variability  
of Evolved Stars  
from COBE DIRBE Data**

Beverly J. Smith

*Department of Physics and Astronomy, East Tennessee State University, Box 70652, Johnson  
City, TN 37614*

smithbj@etsu.edu

**ABSTRACT**

For a complete  $12\ \mu\text{m}$  flux-limited sample of 207 IRAS sources ( $F_{12} \geq 150\ \text{Jy}$ ,  $|b| \geq 5^\circ$ ), the majority of which are AGB stars ( $\sim 87\%$ ), we have extracted light curves in seven infrared bands between  $1.25\ \mu\text{m} - 60\ \mu\text{m}$  using the database of the Diffuse Infrared Background Experiment (DIRBE) instrument on the Cosmic Background Explorer (COBE) satellite. Using previous infrared surveys, we filtered these light curves to remove datapoints affected by nearby companions, and obtained time-averaged flux densities and infrared colors, as well as estimates of their variability at each wavelength. In the time-averaged DIRBE color-color plots, we find clear segregation of semi-regulars, Mira variables, carbon stars, OH/IR stars, and red giants without circumstellar dust (i.e.,  $V - [12] < 5$ ) and with little or no visual variation ( $\Delta V < 0.1$  magnitudes). The DIRBE  $1.25 - 25\ \mu\text{m}$  colors become progressively redder and the variability in the DIRBE database increases along the oxygen-rich sequence non-dusty slightly varying red giants  $\rightarrow$  SRb/Lb  $\rightarrow$  SRa  $\rightarrow$  Mira  $\rightarrow$  OH/IR and the carbon-rich SRb/Lb  $\rightarrow$  Mira sequence. This supports previous assertions that these are evolutionary sequences involving the continued production and ejection of dust. The carbon stars are redder than their oxygen-rich counterparts for the same variability type, except in the  $F_{12}/F_{25}$  ratio, where they are bluer. We find significantly larger infrared variations for Mira stars, carbon stars, and OH/IR stars than for the red giants without circumstellar dust, with semi-regulars and irregulars in between, as expected based on their optical variations. Of the 28 sources in the sample not previously noted to be variable, 18 are clearly variable in the DIRBE data, with amplitudes of variation of  $\sim 0.9$  magnitudes at  $4.9\ \mu\text{m}$  and  $\sim 0.6$  magnitudes at  $12\ \mu\text{m}$ , consistent with them being very dusty Mira-like variables. We also present individual DIRBE light curves of a few selected stars. The DIRBE light curves of the semi-regular variable L<sub>2</sub> Pup are particularly remarkable. The maxima at  $1.25$ ,  $2.2$ , and  $3.5\ \mu\text{m}$  occur  $10 - 20$  days before those at  $4.9$  and  $12\ \mu\text{m}$ , and, at  $4.9$  and  $12\ \mu\text{m}$ , another maximum is seen between the two near-infrared maxima.

*Subject headings:* stars: AGB and post-AGB, stars: variable: Miras

## 1. INTRODUCTION AND MOTIVATION

### 1.1. Asymptotic Giant Branch Stars and Infrared Emission

Asymptotic giant branch (AGB) stars are in the last stage of stellar evolution before becoming planetary nebulae, and are generally surrounded by circumstellar dust shells. AGB stars typically have high rates of mass loss, between  $10^{-8} - 10^{-4} M_{\odot} \text{ yr}^{-1}$  (Knapp & Morris 1985), sometimes losing more than half their mass while on the AGB. These stars return large quantities of carbon-, oxygen-, and nitrogen-enriched gas to the interstellar medium, contributing significantly to the chemical evolution of the Galaxy (Sedlmayr 1994). AGB stars include classical Mira variables (visual amplitudes  $\geq 2.5$ ; periods  $\geq 100$  days), semiregular SRa stars (amplitudes  $\leq 2.5$ ; periods 35 – 1200 days), semiregular SRb stars (amplitudes  $\leq 2.5$ ; with poorly defined periods), and irregular variables (type Lb), as well as dust-enshrouded carbon stars and OH/IR stars. AGB stars can be divided into two main groups depending upon their chemistry, oxygen-rich and carbon-rich. Stars begin their lives on the AGB as oxygen-rich and some, but not all, later become carbon-rich because of carbon dredge-up from their core (Iben & Renzini 1983; Chan & Kwok 1990).

To better understand the mass loss process in AGB stars and the evolutionary relationship between the different types of AGB stars, mid- and far-infrared studies are vital. At wavelengths longer than  $\sim 3 \mu\text{m}$ , emission from dust in the circumstellar envelopes of AGB stars becomes important (Woolf & Ney 1969). Infrared observations have proven useful in constraining models of the circumstellar envelopes of these stars, as well as estimating mass loss rates (e.g., Jura (1986), Bedijn (1987); Anandarao, Pottasch, & Vaidya (1993)). Such studies have provided important clues to the dust properties, temperatures, and distributions in these envelopes.

A common method of distinguishing between AGB stars and other sources is segregation in IRAS color-color plots (e.g., Thronson et al. (1987), Van der Veen & Habing (1988), Ivezić & Elitzur (2000)). When IRAS data are combined with shorter wavelength infrared data, this segregation is improved and it is possible to separate the different types of AGB stars. For example, Ivezić & Knapp (2000) were able to separate SRb/Lb stars from Miras, and oxygen-rich AGB stars from carbon-rich AGB stars, by their location in the  $25 \mu\text{m} - 12 \mu\text{m}$  vs.  $12 \mu\text{m} - \text{K}$  color-color plot. Adding  $3.5 \mu\text{m}$  data improves the segregation: the  $\text{K} - \text{L}$  vs.  $[\text{12}] - [\text{25}]$  and  $\text{K} - \text{L}$  vs.  $\text{L} - [\text{12}]$  color-color diagrams are particularly useful in segregating different types of objects (Epchtein et al. 1987; Guglielmo et al. 1993). Such infrared color-color plots have provided clues to possible evolutionary connections between the different types of AGB stars (e.g., Kerschbaum & Hron (1992), Van der Veen & Habing (1988), Van der Veen (1989), Willems & de Jong (1988), Chan & Kwok (1990), Jones et al. (1990), Marengo, Ivezić, & Knapp (2001)).

Many of the early studies of the circumstellar shells of AGB stars were based on time-averaged mid- and far-infrared data (for example, Jura (1986), Anandarao, Pottasch, & Vaidya (1993)). A large fraction of AGB stars, however, are variable at visible and near-infrared wavelengths, and may well be variable at longer wavelengths as well, causing some uncertainty in these results.

Measurements of variability at longer infrared wavelengths provide much stronger constraints of these models. For example, a number of studies have shown that, for Mira variables, the amplitude of variation tends to decrease with increasing wavelength, from the optical to the mid-infrared (Lockwood & Wing 1971; Harvey et al. 1974; Le Bertre 1992, 1993; Little-Marenin, Stencel, & Staley 1996; Smith et al. 2002). Comparisons of mid-infrared light curves with those in the visible and near-infrared provide information about how the circumstellar shell changes in response to changes in the star. Interesting phenomena such as wavelength-dependent phase lags, where the light curve maximum occurs at different times at different wavelengths, and secondary maxima in the light curves, can provide important additional constraints on models of AGB stars and their circumstellar dust shells.

## 1.2. The COBE DIRBE Mission and Infrared Light Curves of Variable Stars

Most mid-infrared light curves obtained to date are relatively poorly-sampled, making measurements of amplitudes, phase lags, and secondary maxima difficult. To address these issues, in Smith et al. (2002), we recently explored the use of archival data from the Diffuse Infrared Background Experiment (DIRBE) (Hauser et al. 1998) on the Cosmic Background Explorer (COBE) satellite (Boggess et al. 1992) for extracting infrared light curves of Mira variable stars. DIRBE operated for 10 months in 1989-1990, providing full-sky coverage at 10 infrared wavelengths (1.25, 2.2, 3.5, 4.9, 12, 25, 60, 100, 140, and 240  $\mu\text{m}$ ). Although DIRBE was designed to study the cosmic infrared background, its data are also useful for studying point sources, in spite of its relatively poor spatial resolution ( $0.7^\circ$ ). To date, however, stellar fluxes from DIRBE have been little utilized, except for our Mira study and for calibration verification during the DIRBE mission (Burdick & Murdock 1997; Cohen 1998).

DIRBE provided excellent temporal coverage, allowing careful investigation of possible infrared variability of stars. In the course of a week, a typical point on the sky was observed 10-15 times by DIRBE, and over the course of the cryogenic mission, it was observed about 200 times (Hauser et al. 1998). The DIRBE coverage varied with position on the sky. Near the ecliptic poles, sources were generally observed approximately twice a day for the entire mission, giving a total of 400 – 1000 observations over the 10 month mission. Near the ecliptic plane, sources were typically observed roughly twice a day for 2 months, then were inaccessible for 4 months, before coming back into view. For comparison, the Infrared Astronomical Satellite (IRAS) typically provided only two or three independent flux measurements of a star at 12  $\mu\text{m}$  (Little-Marenin & Stencel 1992), while the infrared Midcourse Space Experiment (MSX) mission (Price et al. 1999) made up to six observations over a four month period (Egan et al. 1999).

In our earlier study (Smith et al. 2002), we started with the samples of Sloan & Price (1998) and Sloan, Little-Marenin, & Price (1998). These samples were obtained by cross-referencing the General Catalogue of Variable Stars (Kholopov et al. 1985-1988) with the IRAS Point Source Catalog (1988) and selecting sources with IRAS Low Resolution Spectroscopy available. We then

selected a subset of 38 stars from this sample, with an IRAS  $12\ \mu\text{m}$  flux density cutoff of 235 Jy and classification as Mira stars. This study proved that high quality  $1.25\ \mu\text{m} - 25\ \mu\text{m}$  light curves of infrared-bright stars are obtainable from the DIRBE dataset. In general, the highest S/N light curves are at  $3.5\ \mu\text{m}$  and  $4.9\ \mu\text{m}$ , with decreasing S/N at longer wavelengths. This study confirmed and extended previous results on decreasing amplitudes of variation with increasing wavelengths. In addition, we found evidence for phase lags of the near-infrared maximum relative to that in the visual, and offsets in the times of the mid-infrared maxima relative to those in the near-infrared. The mid-infrared maxima occurred  $\sim 0.05$  phase before those in the near-infrared, but  $\sim 0.05$  phase after those in the optical. In addition, in three stars, clear secondary maxima in the rising portions of their light curves are seen simultaneously in the optical, near-infrared, and mid-infrared, supporting the hypothesis that they are due to shocks rather than newly formed dust layers.

In our earlier study, we specifically targeted AGB stars that were previously known to be Mira variables. This means that we neglected non-Mira AGB stars (semi-regular variables and irregular variables), Miras not previously classified as Miras, and very dust-enshrouded AGB stars without bright optical counterparts. In our current study, we have extended this work to these other types of AGB stars and have increased the sample size to 207. In this paper, we discuss the time-averaged DIRBE colors of the different types of AGB stars, as well as statistical results on infrared variability.

## 2. The Sample and Some Statistics

For this new study, instead of selecting our stars from the Sloan & Price (1998) and Sloan, Little-Marenin, & Price (1998) samples, which were specifically chosen to include only known variables, we have started with a more general infrared-selected sample of stars. For DIRBE variability studies, the best wavelength to use would be  $4.9\ \mu\text{m}$  or  $3.5\ \mu\text{m}$ , since these give the highest S/N DIRBE light curves for AGB stars (Smith et al. 2002). Unfortunately, however, no complete all-sky survey has been made at these wavelengths so far. We therefore use the IRAS  $12\ \mu\text{m}$  band to select our sources, selecting all IRAS sources with  $F_{12} \geq 150$  Jy and  $|b| \geq 5^\circ$ . This is the average  $5\sigma$   $12\ \mu\text{m}$  noise level in the light curves obtained from the DIRBE Calibrated Individual Observations (CIO) database (Smith et al. 2002).

The Galactic latitude limit was chosen to minimize confusion because of the large DIRBE beam ( $0.7^\circ$ ). At the DIRBE  $12\ \mu\text{m}$   $5\sigma$  limit of 150 Jy, the IRAS source counts show that there is on average 0.065 sources per square degree at  $|b| = 5^\circ$ . This corresponds to 28 DIRBE beams per source and a confusion noise of 28 Jy, giving a S/N of 5 at 150 Jy. Thus at higher flux limits and higher Galactic latitudes, confusion is expected to be less important.

Our full sample contains 207 sources. All but six of the sources in the Smith et al. (2002) study are included in the new sample; the remaining six did not meet the Galactic latitude requirement.

Our sample is listed in Table 1<sup>1</sup>, along with information about possible optical counterparts to the IRAS sources from the SIMBAD database (Wenger et al. 1996) and Kwok, Volk, & Bidelman (1997), including optical spectral type and the IRAS spectral classification. We also identify stars known to be OH/IR stars with 1612 MHz OH satellite line emission (from the compilation of Chen et al. (2001)), as well as objects identified as HII regions, planetary nebulae, and post-AGB stars in SIMBAD. Of the 207 sources in our sample, 29 are in the Chen et al. (2001) compilation of OH/IR sources.

In Table 1, we also include information about the variability type, when available. At least 179 of the sources in the sample (86%) are known or suspected from previous studies to be variable. Cross-correlating with the GCVS (Kholopov et al. 1985-1988), we find 158 matches. An additional 20 sources not in the GCVS are included in the New Catalogue of Suspected Variable Stars (Kukarin et al. 1982) or the NSV Supplement (Kazarovets & Durlevich 1998). Some statistics on the variability types of the sample sources are given in Table 2, where the variability type is compared to optical type. Of the previously-known variable sources in the sample, 82 are classified as Miras, 7 are semi-regular type SRa, 39 are SRb stars, 6 are SRc stars, three are unspecified semi-regulars, 15 are type Lb, two are Lc stars, one is an unspecified type L star, one is a symbiotic Z And-type+semi-regular binary pair, one is a possible type R variable (binary with strong reflection of light from hot star on companion), one is an eclipsing binary, and one is a suspected irregular eruptive variables of type IN (Orion variable; likely a pre-main sequence object). The rest are unclassified variables.

All 207 sources in the sample are in the Kwok, Volk, & Bidelman (1997) IRAS Low Resolution Spectra (LRS) catalog sample. The IRAS spectral types given in Table 1 are from Kwok, Volk, & Bidelman (1997), who classified the IRAS spectra according to the scheme of Volk & Cohen (1989). Some statistics on these IRAS spectral types are summarized in Tables 3 and 4, where they are compared with the optical spectral types and the variability types. The IRAS types indicate that at least 171 (82%) of our 207 sample sources are likely dusty evolved stars (LRS types A, C, E, or F). This includes 46 (22% of the sample) carbon-rich stars (type C, with strong 11.2  $\mu\text{m}$  SiC emission), 106 (51%) oxygen-rich stars with 9.7  $\mu\text{m}$  silicate emission (type E), one oxygen-rich star with the silicate feature in absorption (type A), and 18 (9%) type F stars (featureless IRAS spectra that are flatter than expected from a stellar photosphere, indicating small amounts of dust). In addition, 27 sources (13%) have class S LRS spectra, meaning a Rayleigh-Jeans photospheric spectrum with little to no dust. Finally, four sources are type H (generally planetary nebulae, reflection nebulae, or HII regions), one object is type I (noisy or incomplete spectrum), two are type P (red 13 – 23  $\mu\text{m}$  spectra, and a sharp rise at the blue end of the LRS range), while two are type U (unusual spectra that do not fit the other classes).

As noted by Kwok, Volk, & Bidelman (1997) and as seen in Table 3, the optical spectral type

---

<sup>1</sup>Table 1 is only available in electronic form, at the Astronomical Journal web site <http://www.journals.uchicago.edu/AJ/> or at <http://www.etsu.edu/physics/bsmith/dirbe/>

(carbon vs. oxygen-rich star) is strongly correlated with the dust spectral type, as seen in the IRAS mid-infrared Low Resolution Spectra (LRS) database, in that carbon stars tend to show  $11\ \mu\text{m}$  SiC emission, while M-type AGB stars tend to have the  $9.7\ \mu\text{m}$  silicate feature. The LRS type A star is an M star, as are all of our LRS type E stars, with the exception of two optical type S stars ( $\text{C/O} \sim 1$ ) and 11 stars with no optical types. Of the M stars with LRS type E, two are luminosity class II stars and three are SRc variables, thus are likely massive stars rather than AGB stars. The LRS type C stars either have no optical spectral type or are carbon stars, with the exception of one M star. The LRS type F stars are all class M stars (including one M supergiant), except for one K giant. Of the LRS type S stars, 5 are supergiants, one is a carbon star, and 21 are giants. Three of the four LRS class H sources are HII regions or are associated with star formation regions, and the other is a planetary nebula. The LRS type I source is a semi-regular M giant, while one of the LRS class U stars is a carbon Mira and the other is a K supergiant. One of the LRS class P sources is a post-AGB star while the other is associated with a star formation region.

In Table 1, we also include the V magnitude range, if available from one of the three variable star catalogues cited above. Otherwise, if possible, we include the V magnitude given in SIMBAD. A total of 155 of our 207 sources have V magnitudes available. In Figure 1, a histogram of  $V - [12]$  for these 155 stars is given. The shaded region marks the 27 stars with IRAS spectral types of S (dominated by photospheric emission). As expected, these are the bluest stars in the sample in  $V - [12]$ . For comparison, note that a cool M star with a blackbody spectrum is expected to have  $V - [12] \leq 7$  (Cohen et al. 1987). Note, however, that almost all of the LRS type S stars in our sample are known from previous studies to be variable (see Table 4), although none have the large amplitudes that characterize Miras. A star at our  $12\ \mu\text{m}$  flux limit with  $V = 10$  has a  $V - [12] = 11.8$ ; thus this plot is likely incomplete at  $V - [12]$  higher than this.

To search for trends in the infrared colors and variability of the different types of AGB stars, we have divided our sample stars into 26 groups (see Table 6), separating according to the different variability types (Miras, SRa, SRb, SRc, Lb, Lc, sources noted only as ‘variable’ in the GCVS or NSV, and sources not previously classified as variable). We distinguished between carbon stars, oxygen-rich stars, and S stars, and separated out sources known to be OH/IR stars. We also separated out known non-carbon luminosity class I and II stars, since these are likely to be massive stars, and therefore not on the AGB. Luminosity classes and/or variability types are not available for all of the stars in the current study, however, since supergiants are rare and main sequence stars have low luminosities, we assume that if this information is not available the star is probably a giant star.

The non-supergiant oxygen-rich sources with unspecified variability are an inhomogeneous group, containing both optically-faint stars without many optical or near-infrared measurements, and well-studied optically-bright stars with small variations. To separate these two categories of stars, we further sub-divided this group by  $V - [12]$ . There are six optically-bright ( $V < 3.5$ ) very blue ( $V - [12] < 5$ ) K and M giants in this group which are slightly variable at optical wavelengths ( $\sim 0.1$  magnitudes in V). In contrast, the other five unspecified non-supergiant variables are very

red, with  $V - [12] > 13.5$ , or have no  $V$  magnitudes available (i.e.,  $V - [12]$  likely  $> 12$ ). These two groups are separated in Table 6, since they are likely in different evolutionary stages. In addition, there is one optically-bright ( $V = 2.23$ ) very blue star ( $V - [12] \sim 4.1$ ) non-variable star,  $\gamma$  Dra, in the oxygen-rich stars without variability information group. This star is in marked contrast to the rest of the oxygen-rich stars with no variability information, which have no  $V$  magnitudes available. Thus  $\gamma$  Dra is separated out into a different group. Also, the single known eclipsing binary in the sample, the optically-bright ( $V = 1.9$ ) star  $\epsilon$  Car, which contains a K3 III star, is very blue ( $V - [12] \sim 4.25$ ) with an LRS spectral type of S, and shows no signs of variability in the DIRBE data. Thus this is grouped with  $\gamma$  Dra. These eight optically-bright non-variables and slightly variable stars are likely not AGB stars, but rather red giant branch or red clump stars.

Of the 207 sources in our full sample, 180 (87%) are likely AGB stars, based on their optical and IRAS spectral types. Of the remainder, four are associated with star formation regions, 13 are non-carbon supergiants, bright giants, and/or SRc variables (and therefore likely massive stars), one is a post-AGB star, one is a planetary nebula, and 8 are likely giant branch or red clump stars.

### 3. The COBE Data

In Table 5, the time-averaged DIRBE flux densities in the six shortest wavelength DIRBE bands are given<sup>2</sup>. These values were extracted from the DIRBE CIO database using software written by Nils Odegard. The CIO database contains the calibrated individual 1/8th second samples taken in science-survey mode during each day of the DIRBE cryogenic mission. For all scans that pass within  $0.3^\circ$  of the target position, a linear baseline is fit to the sections  $\pm 1.35^\circ - 2.25^\circ$  from the point of closest approach. The point source photometry is obtained by subtraction of this baseline and correcting for DIRBE beam response. The uncertainties in the point source photometry are calculated as the quadrature sum of the rms noise of the baseline, an error due to positional uncertainties of  $1'$  in both the in-scan and cross-scan directions, an error due to short-term detector gain variations, and signal-dependent detector noise. The average noise levels per individual flux measurements are 25, 20, 20, 10, 30, 55, 320, 765, 4800, and 2750 Jy for the DIRBE 1.25 – 240  $\mu\text{m}$  filters, respectively.

To test for possible contributions to the DIRBE 12, 25, and 60  $\mu\text{m}$  flux densities from infrared-bright stars near the targeted sources, we have searched the IRAS Point Source Catalog for additional infrared-bright sources within  $0.5^\circ$  of the target source. At 12, 25, and 60  $\mu\text{m}$ , 4, 2, and 2 sources in our list, respectively, had nearby sources within  $0.5^\circ$  above the COBE  $1\sigma$  noise levels for individual flux measurements given above. These objects are flagged in Table 5. The two sources flagged at 25 and 60  $\mu\text{m}$  are both star formation regions, one of which is also flagged at 12  $\mu\text{m}$ .

---

<sup>2</sup>Table 5 is only available in electronic form, at the Astronomical Journal web site at <http://www.journals.uchicago.edu/AJ> or at <http://www.etsu.edu/physics/bsmith/dirbe/>

As an additional test for confusion, for our sample sources we compared the time-averaged DIRBE 12, 25, and 60  $\mu\text{m}$  flux densities with the IRAS Point Source Catalog flux densities. Greater than  $3\sigma$  disagreements were found for 5, 24, and 13 sources at 12, 25, and 60  $\mu\text{m}$ , respectively. These sources are also flagged in Table 5. These flagged objects include all four of the H II regions in the sample as well as the planetary nebula. A few evolved stars are also flagged. A few of these flagged evolved stars have been found to be extended at 60 and 100  $\mu\text{m}$  in the IRAS data (Hawkins 1989, 1990a,b; Young, Phillips, & Knapp 1993a,a), however, in all but the case of  $\alpha$  Ori the DIRBE flux densities are significantly larger than the total IRAS flux densities, suggesting additional sources of confusion.

At 1.25 and 2.2  $\mu\text{m}$ , we use the all-sky Two Micron All Sky Survey (2MASS)<sup>3</sup> (Cutri et al. 2003) to check for additional bright sources in the DIRBE beam. At 1.25 and 2.2  $\mu\text{m}$ , respectively, 6 and 58 sources were flagged as having a companion within  $0.5^\circ$  above the DIRBE noise level. At 3.5 and 4.9  $\mu\text{m}$ , no all-sky surveys are available. At these wavelengths, to check for possible additional sources in the DIRBE beam, we used the Catalog of Infrared Observations (Gezari, Pitts, & Schmitz 1999)<sup>4</sup>, a compilation of all published infrared observations available in 1997. At 4.9  $\mu\text{m}$ , we also used the synthetic all-sky 4.2  $\mu\text{m}$  catalog of Egan & Price (1996), which was created by extrapolation from the IRAS catalogues, other infrared catalogues, and optical measurements. A total of 3 sources were flagged as having companions above the DIRBE noise levels at 3.5  $\mu\text{m}$  in the DIRBE beam, while 24 sources were flagged at 4.9  $\mu\text{m}$ . We note that these catalogs may be incomplete, even at these very bright limits, thus these are lower limits to the numbers of confused sources at these wavelengths.

Another issue is the possibility of more distant companions affecting the ‘sky’ fluxes used in the CIO photometry. Careful inspection of the DIRBE data showed that, if a second infrared-bright star is between about  $0.5^\circ - 2.5^\circ$  of the target star, then for scans that passed through the nearby star, flux from the companion star sometimes contributed significantly to the ‘sky flux’ used in the DIRBE point source photometry routine, causing erroneous photometry with large errorbars for the targeted star. Fortunately, however, scans in other directions were not affected by the second star. To correct for this problem, we filtered our data to remove affected scans. At 12, 25, and 60  $\mu\text{m}$ , we searched the IRAS Point Source Catalog for objects within  $3.2^\circ$  of each targeted source. At each wavelength, for each DIRBE scan for each targeted source, we scaled the IRAS flux densities of the nearby stars by a Gaussian with FWHM  $0.7^\circ$ , weighted by the minimum distance between the scan and the companion star. If the weighted IRAS flux density in the respective band was greater than the DIRBE noise limit, then the scan was removed from consideration. This technique dramatically improved the DIRBE light curves of some stars, removing discrepant data points and those with large errorbars. At 12, 25, and 60  $\mu\text{m}$ , respectively, 71, 24, and 7 of our sources had some scans affected by a bright companion. We note that some uncertainty still remains, since

---

<sup>3</sup><http://www.ipac.caltech.edu/2mass/>

<sup>4</sup>Available from the VizieR service at <http://vizier.u-strasbg.fr/viz-bin/VizieR>



this process does not take into account the possibility that the infrared brightnesses of some of the nearby stars may change with time.

In a few cases, the nearby sources are extended, and, although the source clearly affects some of the DIRBE scans, the Point Source Catalogue fluxes are below our cut-off. To test for these cases, we also searched in the IRAS Small Scale Structure Catalog (Helou & Walker 1985) for companions above our flux cutoff, and filtered the DIRBE data accordingly. At 12, 25, and 60  $\mu\text{m}$ , only 1, 10, and 11 sources respectively were affected by such companions.

At 1.25 and 2.2  $\mu\text{m}$ , we used the 2MASS database to filter the data, while at 3.5  $\mu\text{m}$ , we used the Catalog of Infrared Observations, and at 4.9  $\mu\text{m}$ , we used both the Catalog of Infrared Observations and the Egan & Price (1996) catalog. At 1.25  $\mu\text{m}$ , 2.2  $\mu\text{m}$ , 3.5  $\mu\text{m}$ , and 4.9  $\mu\text{m}$ , 82, 205, 56, and 193 out of our 207 sources had at least some scans potentially affected by a nearby companion.

In some cases, this filtering dramatically improved the light curves (see Figure 2). However, because of incompleteness in the comparison catalogs and the fact that some of the nearby stars may themselves be variable, this filtering is sometimes not perfect. Also, at our brightness levels, the 2MASS observations were saturated, so the photometry is relatively inaccurate ( $\sim 0.2 - 0.3$  magnitudes; Cutri et al. (2003)), which introduces some additional uncertainty into the filtering process. We therefore inspected each final filtered light curve by eye, looking for obvious evidence for companions (as in Figure 2). These light curves were also flagged in Table 5.

These filtering routines cannot correct for cosmic ray hits, which can also cause anomalous points in the DIRBE light curves. The remaining datapoints with large error bars ( $\geq 3$  times the average uncertainty) were likely affected by a cosmic ray hit in the ‘sky’ portion of the light curve, and so were removed from the light curves by an additional filtering process. Generally, only a few DIRBE datapoints per light curve were removed by this additional filtering processing.

We note that a cosmic ray hit near the star itself may not cause a large error bar, but instead may simply manifest itself as a very discrepant flux measurement with a small error bar. The typical time resolution of the DIRBE data is  $\sim 9$  hours, thus a true rapid variation of the star would show the same signature. Large amplitude visual variations (0.5 – 1 magnitude) with timescales of hours or days have been claimed on the basis of Hipparcos data (de Laverny et al. 1998) (but see Kerschbaum, Lebzelter, & Lazaro (2001)). To look for such events in the DIRBE data, we compared the flux in a single measurement with the mean of the closest six measurements in time. Points that differed by greater than  $5\sigma$  were then inspected individually. In none of the unconfused sources did such a large deviation occur at three or more DIRBE wavelength simultaneously, strongly indicating that these points are caused by cosmic rays rather than real variations. We therefore removed these points from the light curves for the following variability analysis.

In addition to the time-averaged infrared flux densities, Table 5 also includes both the standard deviation of the individual flux values in the light curve of the object (after filtering), along with the mean uncertainty of the individual data points in the light curve. The comparison of these

two values provides an estimate of the likelihood of variability of the object (See Section 5.2). The standard error of the mean is also provided, along with the number of data points (sightings) for the objects after the final filtering. In addition, the observed amplitude of variation at each wavelength (see Section 4.2) is also included in Table 5.

No color corrections have been applied to the data in Table 5. To investigate the uncertainties associated with color corrections, we created lookup tables of expected observed flux density ratios for adjacent DIRBE bands for a large range of blackbody temperatures, using  $\lambda^0$ ,  $\lambda^{-1}$ , and  $\lambda^{-2}$  emissivity laws and integrating over the DIRBE responsivities. Comparison with the observed DIRBE flux ratios for the sample stars yielded equivalent temperatures. For each DIRBE band except 1.25  $\mu\text{m}$  and 25  $\mu\text{m}$ , the average of the two temperatures obtained from comparison with the two adjacent bands were used with the DIRBE color correction tables (Hauser et al. 1998) to estimate color corrections. At 1.25  $\mu\text{m}$  and 25  $\mu\text{m}$ , only the temperatures implied by the 1.25  $\mu\text{m}/2.2 \mu\text{m}$  and 12  $\mu\text{m}/25 \mu\text{m}$  ratios, respectively, were used. At 3.5, 4.9, 12, and 25  $\mu\text{m}$ , the implied corrections were quite small, typically  $\leq 5\%$ , differing by a few percent depending upon the assumed emissivity law. At 1.25  $\mu\text{m}$  and 2.2  $\mu\text{m}$  the implied color corrections were somewhat larger, up to  $\sim 10\%$ , differing by up to  $\sim 5\%$  with the different emissivity laws. Since the color corrections are small, and the uncertainty associated with the emissivity law is on the same order as the color corrections themselves, we elected to not include color corrections in the following analysis.

In Figures 3 and 4, we show some representative final filtered light curves of different types of stars. These stars are discussed below.

## 4. RESULTS

### 4.1. Time-Averaged Infrared Color-Color Plots

In Figures 5 – 8, we present the time-averaged DIRBE color-color diagrams for the stars in our sample, using the six shortest wavelength DIRBE bands. In these plots, we have excluded sources flagged in Table 5 at at least one of the relevant wavelengths. We also excluded the star formation regions, planetary nebulae, post-AGB sources, and the symbiotic binary. For clarity, we have also excluded sources likely to be massive stars (luminosity classes I and II, variability types SRc and Lc).

In Table 6, we provide the mean colors and rms spread for our 26 groups of stars. These results are summarized in Figures 9 and 10, where we plot the average colors for the different types of AGB stars, along with their dispersions. For comparison with these plots and tables, note that  $J - K = -2.5 \log (F_{1.25}/F_{2.2}) + 0.98$  and  $K - L = -2.5 \log(F_{2.2}/F_{3.5}) + 0.89$  (Bessell & Brett 1988), while  $[12] - [25] = -2.5 \log (F_{12}/F_{25}) + 1.56$  (Beichman et al. 1988), though filter differences and color corrections may cause slight differences.

These color-color plots, along with Table 6, show a clear segregation of different types of

objects. The semi-regulars are bluer than Miras on average, with Miras known to be OH/IR stars being redder than oxygen-rich Miras not classified as OH/IR stars. Carbon-rich Miras are redder than oxygen-rich Miras in general, and carbon-rich stars not previously classified as Miras are also very red. Among the semi-regulars, the SRa stars are redder than the SRb stars. Among the known OH/IR stars, there is a trend, in that the known semi-regulars are bluest, objects without a specified variability type are reddest, and Miras are in between. The bluest colors belong to the optically-bright red giants with little or no visual variations (for example,  $\beta$  And,  $\alpha$  Hya,  $\alpha$  Boo, and  $\beta$  UMi), all of which are IRAS LRS type S (dominated by photospheric emission in the IRAS spectra). These stars likely are not yet AGB stars.

For the 155 stars with V measurements, in Figures 11 and 12, we compare  $V - [12]$  with the four shortest wavelength DIRBE colors. Note that these plots are likely incomplete above  $V - [12] \sim 11.8$ . As expected, in most cases, the DIRBE colors get redder as  $V - [12]$  gets redder. However, note that for the oxygen-rich stars  $F_{3.5}/F_{4.9}$  gets bluer as  $V - [12]$  reddens to  $V - [12] \sim 7$ , then the trend reverses. Note also that, for a given  $V - [12]$ , the carbon stars are redder in  $F_{1.25}/F_{2.2}$  and  $F_{2.2}/F_{3.5}$  than the oxygen-rich stars. In the  $V - [12]$  vs.  $F_{3.5}/F_{4.9}$  and  $F_{12}/F_{25}$  plots, the carbon and oxygen-rich stars are indistinguishable.

## 4.2. DIRBE Variability

For each light curve with minimum flux density greater than five times the typical DIRBE noise level for that wavelength, we have calculated the total *observed* change in brightness during the DIRBE observations, after averaging over one week time intervals. We note that these observed changes in brightness do not necessarily represent the full range of variation for these stars, because many of the light curves are not complete and may not cover a full pulsation period. In these cases, the observed variations are a lower limit to the true amplitudes of variation. Of the unflagged sources, excluding sources with less than  $5\sigma$  DIRBE flux densities at minimum light, at 1.25, 2.2, 3.5, 4.9, 12, and 25  $\mu\text{m}$ , respectively, 81, 107, 103, 138, 96, and 47 stars have  $>3\sigma$  detections of variability (i.e.,  $\Delta(\text{mag})/\sigma_{\Delta(\text{mag})} > 3$ ), and 57, 89, 79, 106, 66, and 28 stars have  $\geq 5\sigma$  detections of variability. One star, the carbon star CW Leo (IRC +10216), has greater than  $3\sigma$  variation at 60  $\mu\text{m}$  and 100  $\mu\text{m}$ . It varies by  $1.63 \pm 0.05$ ,  $1.47 \pm 0.04$ ,  $1.17 \pm 0.01$ ,  $0.82 \pm 0.02$ ,  $0.67 \pm 0.02$ ,  $0.49 \pm 0.05$ , and  $0.43 \pm 0.07$  magnitudes at 2.2, 3.5, 4.9, 12, 25, 60, and 100  $\mu\text{m}$ , respectively (see Figures 3A – E).

In Figures 13 – 18, we present histograms of these observed variations, in magnitudes, for the 26 groups of stars in our sample. The average observed amplitude of variation at each wavelength,  $\langle \Delta(\text{mag}) \rangle$ , in magnitudes, for these 26 groups, is given in Table 7, along with the rms spread. To demonstrate the significance of  $\langle \Delta(\text{mag}) \rangle$ , in Table 7 we also include the average uncertainty in  $\Delta(\text{mag})$ ,  $\langle \sigma(\Delta(\text{mag})) \rangle$ . In constructing Table 7 and Figures 13 – 18, we only included stars with  $>5\sigma$  DIRBE flux densities at minimum light.

Miras show significantly larger variations in the DIRBE data than the semi-regulars, and the SRa’s have larger variations than the SRb’s. The Miras have average observed amplitudes of  $\sim 1$  magnitude at  $1.25 \mu\text{m}$  and  $\sim 0.6$  magnitudes at  $4.9 \mu\text{m}$ , while the non-massive SRa’s and SRb’s have average observed amplitudes of 0.41 and 0.17 magnitudes at  $1.25 \mu\text{m}$  and 0.15 and 0.09 magnitudes at  $4.9 \mu\text{m}$ , respectively.

In Figures 3F – P and 4A – B, we show some example light curves for a few Miras and semi-regular stars. Note the inflection point in the rising portion of the  $4.9 \mu\text{m}$  light curves of the Mira variables T Dra and R Vol (Figures 3F and 3H). Such inflection points have been noted before in the mid-infrared light curves of Miras (Smith et al. 2002). Note also the striking difference between the  $1.25 \mu\text{m}$  and  $4.9 \mu\text{m}$  light curves for the oxygen-rich SRb star L<sub>2</sub> Pup. The maxima at  $1.25 \mu\text{m}$  precede those at  $4.9 \mu\text{m}$  by 10 – 20 days. Also, at  $4.9 \mu\text{m}$ , a secondary peak is seen between the two  $1.25 \mu\text{m}$  maxima. The  $2.2 \mu\text{m}$  and  $3.5 \mu\text{m}$  light curves (not shown) resemble the  $1.25 \mu\text{m}$  curve, while the  $12 \mu\text{m}$  curve (not shown) is similar to that at  $4.9 \mu\text{m}$ .

The least variable stars in the sample are the optically-bright giants without circumstellar dust ( $V - [12] < 5$ ) (including both the stars known to vary slightly in the optical and the stars with no known variability). These stars have essentially no observed variations in the DIRBE data ( $3\sigma$  upper limits  $< 0.03 - 0.1$  magnitudes; Table 7; see for example Figure 4C and D). In contrast, the optically-faint stars not previously classified as variable are quite variable in the DIRBE data, varying by  $\sim 0.9$  magnitudes at  $4.9 \mu\text{m}$ , even more than the classified Miras (no information is available at  $1.25 \mu\text{m}$ , since these stars are too faint at  $1.25 \mu\text{m}$  to measure variations). Inspection of these light curves by eye confirms that, of the 28 stars in our sample not previously known to be variable, 18 are clearly variable in the DIRBE data (see, for example, Figure 4E – H). This boosts the number of known variable stars in our complete  $12 \mu\text{m}$  flux-limited sample from 179 to 197, or 95% of the sample (note, however, that some of the catalogued variables are not observably variable in the DIRBE database). This difference in the observed DIRBE amplitudes of variation of the optically-bright stars ( $V - [12] < 5$ ) and the optically-faint stars ( $V - [12] > 12$ ) in the combined ‘variable’/‘not known to be variable’ class confirms that these are two distinct populations of stars.

Among the variability types, there is a slight tendency for the carbon-rich stars to be more variable than the oxygen-rich stars (Table 7), however, these differences are small and may not be statistically significant.

To investigate how the amplitudes of variation vary with wavelength, in Figure 19a we plot the *observed* amplitude at  $1.25 \mu\text{m}$  against that at  $2.2 \mu\text{m}$ , including only stars with  $5\sigma$  fluxes at minimum brightness at both wavelengths. In Figures 19b, 19c, 19d, and 19e, we plot  $\Delta\text{mag}(2.2 \mu\text{m})$  vs.  $\Delta\text{mag}(3.5 \mu\text{m})$ ,  $\Delta\text{mag}(3.5 \mu\text{m})$  vs.  $\Delta\text{mag}(4.9 \mu\text{m})$ ,  $\Delta\text{mag}(4.9 \mu\text{m})$  vs.  $\Delta\text{mag}(12 \mu\text{m})$ , and  $\Delta\text{mag}(12 \mu\text{m})$  vs.  $\Delta\text{mag}(25 \mu\text{m})$ , respectively. In all five plots, correlations are seen. Inspection of these plots shows that the average amplitude of variation at the longer wavelength in each panel is less than at the shorter wavelength. This is quantified in Table 8, where the mean ratios of the amplitudes at adjacent wavelengths are provided for the different classes of object in the sample.

This tabulation excludes stars with flux densities less than  $5\sigma$  at minimum and with less than a  $5\sigma$  detection of variation at both wavelengths. Although there is significant scatter in Figure 19, in most cases, the average amplitude ratios (Table 8) are greater than one, indicating that the amplitude of variation generally decreases with increasing wavelength. There is a slight tendency for carbon-rich stars to have a larger  $4.9 \mu\text{m}$  to  $12 \mu\text{m}$  ratio than oxygen-rich stars; otherwise, there is little significant difference between the different classes of stars.

Since the DIRBE cryogenic period was relatively short compared to a typical AGB star pulsation period, for most stars it was not possible to determine a period from the DIRBE data. However, for 103 of the likely AGB stars in our sample, periods are available from the GCVS or the NSV. For these stars, in Figure 20 we have plotted the period against the 5 shortest wavelength DIRBE colors. These plots show that, except for  $F_{12}/F_{25}$ , as the period increases, the stars get redder.

## 5. DISCUSSION

### 5.1. Oxygen-Rich Stars

Some clear trends are apparent in the time-averaged DIRBE colors and the infrared variability of the AGB stars in this sample (Tables 6 and 7, and Figures 5 – 18). For oxygen-rich stars on the AGB, the infrared colors become redder and the observed amplitudes of variation increase along the sequence visually-bright slightly-varying non-dusty giants  $\rightarrow$  SRb  $\rightarrow$  SRa  $\rightarrow$  Mira  $\rightarrow$  Mira OH/IR stars  $\rightarrow$  OH/IR stars known to be variable but without a variability classification. At the four shortest wavelengths, the SRb stars are bluer than the SRa’s; from  $4.9 \mu\text{m}$  to  $25 \mu\text{m}$  the colors are indistinguishable. As noted by Kerschbaum & Hron (1992), the V amplitude criteria for Mira selection ( $\Delta(\text{mag}) > 2.5$ ) is not strictly followed in the GCVS, in that some nearby well-studied stars that exceed this limit are classed as SRa or SRb rather than Miras because of irregularities in their light curves. The intermediate infrared colors of the SRa’s between Miras and SRb’s, along with their amplitudes and periods, lead Kerschbaum & Hron (1992, 1994) to conclude that oxygen-rich SRa stars are a mixture of Miras and SRb sources, rather than a unique type of stars. In our sample, both of the carbon SRa’s and two of the three oxygen-rich SRa’s have V ranges in the GCVS greater than 2.5 magnitudes, suggesting that they may be misclassified Miras. We note, however, that their infrared colors are bluer than the majority of Miras.

The infrared colors of the Lb stars are similar to those of the SRb stars, as noted previously by Kerschbaum, Lazaro, & Habison (1996). The DIRBE variabilities of these two classes (Table 7 and Figures 13 – 18) are also similar. Based on a Galactic scale height analysis, Jura & Kleinmann (1992) concluded that irregulars and semi-regulars belong to the same population. A detailed study of long term light curves of Lb and SRb stars by Kerschbaum, Lebzelter, & Lazaro (2001) showed that they are essentially the same class of objects, consistent with our results.

The infrared colors of the optically-faint unspecified oxygen-rich variables in our sample (other than the unspecified OH/IR stars and the supergiants/bright giants) are between those of the Miras and the semi-regulars, suggesting that they are a mixture of those two populations. This conclusion is supported by the distribution of observed amplitudes in these classes (Figures 13 – 18 and Table 7).

The ten optically-faint oxygen-rich stars without previous variability information are very red, similar to the OH/IR Miras and redder than the non-OH/IR Miras. Visual inspection of the DIRBE light curves for these sources suggests that at least some of them are previously unidentified Miras. Six are clearly strongly variable in the mid-infrared, with average amplitudes of variation of approximately 0.75 magnitudes at  $4.9 \mu\text{m}$ , 0.6 magnitudes at  $12 \mu\text{m}$ , and 0.4 magnitudes at  $25 \mu\text{m}$  (for example, see Figures 4E and F). These are consistent with the amplitudes found for the known Miras in the sample. The fact that these very red stars with colors similar to those of OH/IR stars are not known 1612 MHz OH/IR masers suggests that the OH/IR phase may be intermittent (i.e., Lewis (2002)) or that not all very evolved oxygen-rich stars become observable 1612 MHz sources.

In general, for the stars with  $V$  magnitudes available, as  $V - [12]$  gets redder, the DIRBE colors also get redder. For the bluest stars ( $V - [12] < 7$ ), which have little circumstellar dust, the increase in  $V - [12]$  is due to increasing titanium oxide absorption in the visible with decreasing photospheric temperature. For stars with larger  $V - [12]$ , dust absorption also depresses the visible light. Interestingly, for the oxygen-rich stars, for  $V - [12] \leq 7$ , as  $V - [12]$  gets redder,  $F_{3.5}/F_{4.9}$  gets bluer (Figure 11c). This trend reverses at redder  $V - [12]$ , where both colors get redder. This depression in the  $4.9 \mu\text{m}$  flux density for very cold stars without circumstellar dust is probably due to an increase in the  $4.3 - 4.7 \mu\text{m}$  CO absorption in these stars. Spectroscopic observations from the Infrared Space Observatory (ISO) shows that the equivalent width of this absorption band increases strongly with decreasing temperature for normal stars without circumstellar shells (Heras et al. 2002).

Since the DIRBE cryogenic period is shorter than a pulsation period, we are not able to use the DIRBE light curves to accurately determine pulsation periods for these stars. However, by inspection of the DIRBE light curves by eye, for 3 of these 10 stars, we are able to estimate a rough lower limit to the pulsation period for these stars. These lower limits range from 340 to 370 days, showing, as expected, that these very red stars have long pulsation periods.

These trends in infrared colors and variations support a scenario of stellar evolution in which, as stars evolve up the AGB, their pulsation amplitudes, mass loss rates, and opacities increase, and their infrared colors become progressively redder. In this picture, they first evolve from semi-regulars to Miras (Kerschbaum & Hron 1992) and then, depending upon their chemistry, to either extreme carbon stars or OH/IR stars (Van der Veen & Habing 1988; Van der Veen 1989; Chan & Kwok 1990; Jones et al. 1990).

The true evolutionary picture, however, may not be this simple. Of the stars with IRAS colors suggesting a detached shell (i.e., a  $60 \mu\text{m}$  excess) a significant fraction are semi-regulars,

leading Willems & de Jong (1988) to suggest that semi-regulars are transition objects, associated with thermal pulses and dredge-up. However, Ivezić & Elitzur (1995) found that contamination by cirrus may be responsible for most of the observed  $60 \mu\text{m}$  excesses, negating this argument. It is true, however, that some semi-regulars do have very extended envelopes. In their study of circumstellar envelopes resolved in the IRAS database, Young, Phillips, & Knapp (1993a) found that most of the resolved stars are semi-regulars, while most of the unresolved stars are Miras. They conclude that the most likely explanation is that the semi-regulars have been losing mass longer. This suggests that semi-regulars are not always in an earlier evolutionary stage from Miras.

This idea is supported by theoretical modeling of the  $[12] - [25]$  to  $K - [12]$  colors and IRAS spectra of semi-regulars and Miras by Ivezić & Knapp (2000) and Marengo, Ivezić, & Knapp (2001). Their work indicates that semi-regulars lack hot dust in their envelopes, implying a decrease in the mass-loss rate in the last  $\sim 100$  years. Furthermore, very long term light curves of a few variable stars show apparent mode switching, with dramatic changes in their light curves from long-period, high amplitude variations to short-period lower amplitude variations (Bedding et al. 1998). Thus the evolutionary connection between semi-regulars and Miras is still uncertain.

## 5.2. OH/IR Stars

Another complication to the evolutionary scenario outlined above is the fact that it is difficult to distinguish between mass sequences and evolutionary sequences. As noted above, 13 stars in our sample are likely massive stars not on the AGB ( $>6-8 M_{\odot}$  main sequence mass), based on their classification as non-carbon luminosity class I or II stars or variability type SRc or Lc stars. For OH/IR stars, another mass indicator is the velocity separation  $\Delta V$  of the 1612 MHz lines, which is a measure of the expansion velocity of the circumstellar shell. This velocity separation is correlated with galactic latitude and random motion relative to galactic rotation, and is therefore correlated with main sequence mass, with stars with the highest  $\Delta V$  being mainly M supergiants (Baud et al. 1981). In Figure 21, for the OH/IR stars in our sample with  $\Delta V$  values available from Chen et al. (2001), we plot  $\Delta V$  vs. the DIRBE flux ratios for the six shortest DIRBE wavelengths. The star with the largest  $\Delta V$  in our sample by far is VY CMa, the sole known OH/IR supergiant in the sample, with  $\Delta V = 65 \text{ km s}^{-1}$  (Chen et al. 2001). VY CMa is quite variable in the optical, varying between magnitude 6.5 and 9.6 at V (GCVS). It is also somewhat variable in the DIRBE database (see Figures 4I – J), but less so than the Miras, varying by only  $0.16 \pm 0.02$  magnitudes at  $4.9 \mu\text{m}$ ,  $0.10 \pm 0.01$  magnitudes at  $12 \mu\text{m}$ , and  $0.11 \pm 0.01$  magnitudes at  $25 \mu\text{m}$ . After VY CMa, there is a large gap in  $\Delta V$ , with the next largest  $\Delta V$  belonging to the Mira variable WX Psc.

At all wavelengths, a slight correlation is seen in Figure 21, in that the stars become redder as  $\Delta V$  increases. Such a correlation with  $F_{12}/F_{25}$  has been seen before (e.g., Lewis, Eder, & Terzian (1990); Chen et al. (2001)); the DIRBE data show that it is also present at the other infrared wavelengths as well, particularly  $F_{4.9}/F_{12}$ . The existence of an OH maser requires a large dust column density to shield the OH molecules from photodissociation (Huggins & Glassgold 1982). As

discussed by Lewis, Eder, & Terzian (1990), when the expansion velocity is large, dust shielding for the OH molecules is diluted, reducing the OH column density and so the probability of an observable OH maser. Thus for large expansion velocities, only objects with high dust column densities (and therefore redder colors) are seen as OH masers. The bluest OH masers are therefore those with smaller  $\Delta V$ .

Note that, in addition to VY CMa, which stands alone, there appears to be two distinct groups of OH/IR stars present in these plots: those with  $\Delta V \leq 15 \text{ km s}^{-1}$  and those between 20 and  $40 \text{ km s}^{-1}$ , with a gap between the two groups. The colors of the second group, on average, are clearly redder than those in the first group. The fundamental difference between these two groups may be main sequence mass; Baud & Habing (1983) conclude that OH/IR stars with smaller values of  $\Delta V$  ( $\leq 15 \text{ km s}^{-1}$ ) have lower main sequence masses than those with  $\Delta V$  between 20 and  $40 \text{ km s}^{-1}$ .

Another parameter that may be related to main sequence mass is the IRAS spectral type. Volk & Kwok (1988) found that stars with silicate absorption features tend to lie in the Galactic Plane, while silicate emission stars are found at both high and low galactic latitude. In their study of OH/IR stars, Chen et al. (2001) found that the LRS type ‘A’ (absorption) stars mainly lie in the Galactic plane, in contrast to the type ‘E’ (emission) stars. These studies concluded that LRS type ‘A’ stars are more massive than many of the type E stars, and that the LRS types may be a mass sequence, rather than an evolutionary sequence. Within the high mass stars, there may be evolution from LRS type E to A, but lower mass stars do not reach the A stage. This conclusion is reinforced by the study of He & Chen (2001), who found that the type E OH/IR stars appear to have a different luminosity-period relation than the type A OH/IR stars.

The sample studied in the current paper, which is selected to be at relatively high latitude ( $|b| > 5^\circ$ ), only contains one LRS type A source, the unspecified variable OH 338.1+6.4, an M star at  $b = 6.4^\circ$ . This source has a much more moderate  $\Delta V$  than VY CMa,  $26 \text{ km s}^{-1}$ , similar to many of the type E Miras. It is much more variable in the DIRBE database than VY CMa, varying by about 0.6 magnitudes at  $12 \mu\text{m}$  and 0.2 magnitudes at  $25 \mu\text{m}$ , typical of a Mira. Compared to the LRS type ‘E’ stars with similar  $\Delta V$ s (and therefore presumably similar main sequence masses), OH 338.1+6.4 is redder in the DIRBE  $F_{4.9}/F_{12}$  and  $F_{12}/F_{25}$  ratios (Figure 21), suggesting that it may be in a later stage of evolution than the type E stars. Thus this may be evidence for evolution from type E to type A stars within the higher main sequence mass range.

The other two OH/IR stars without a variability class (OH 329.8-15.8 and OH 348.2-19.7) were identified as OH/IR stars by Gaylard et al. (1989), who noted that they are optically invisible and variable in the IRAS database. In the Chen et al. (2001) database, their values of  $\Delta V$  are also moderate,  $29 \text{ km s}^{-1}$  and  $24 \text{ km s}^{-1}$ , respectively. In the DIRBE database, OH 348.2-19.7 is strongly variable, by  $1.11 \pm 0.08$  magnitude at  $4.9 \mu\text{m}$  and  $1.20 \pm 0.16$  magnitudes at  $12 \mu\text{m}$  (Figures 4K and L). In contrast, OH 329.8-15.8 is only marginally variable in the DIRBE database ( $0.31 \pm 0.07$  magnitude at  $4.9 \mu\text{m}$  and  $0.25 \pm 0.08$  magnitudes at  $12 \mu\text{m}$ ; see Figures 4M and N).



Recent work by Lewis (2002) has called into question the idea that OH/IR stars are always very evolved stars in the last stage of evolution before becoming planetary nebulae. His follow-up study of 328 stars previously detected in the 1612 MHz OH line yielded four non-detections, implying that those four stars are now ‘dead’ OH/IR stars: the 1612 MHz line has disappeared. Since these stars still have other characteristics of AGB stars, this implies that stars pass through the OH/IR phase more than once. A thermal pulse may trigger a short period of heavy mass loss, sufficient to allow temporary OH maser activity. In this scenario, relatively blue  $F_{12}/F_{25}$  colors are expected (Lewis 2002).

Our sample contains two OH/IR stars, U Men and R Crt, which are classified as semi-regulars rather than Miras. They have relatively low values of  $\Delta V$  (8 and 20 km s<sup>-1</sup>, respectively; Chen et al. (2001)). Their infrared colors similar to those of other semi-regulars (see Table 6) and are also similar to OH/IR Miras with similarly-low values of  $\Delta V$  (Figure 21). The redder of these two stars, the SRa star U Men, has a Mira-like  $V$  amplitude of 2.9 and a relatively long period of 407 days (GCVS), and  $\Delta V$  of  $\sim 20$  km s<sup>-1</sup> (Chen et al. 2001), in the gap between the low mass and higher mass stars. It also varies strongly in the infrared (see Figures 3L and M). The bluer star, the SRb star R Crt, has a  $V$  amplitude of only 1.4 and a much shorter period of 160 days (GCVS), and has a small  $\Delta V$  of 8 km s<sup>-1</sup> (Chen et al. 2001). R Crt is included in the Chen et al. (2001) catalog based on the possible detection by Dickinson, Bechis, & Barrett (1973) of a weak 2 Jy 1612 MHz OH line. However, Etoke et al. (2001) were not able to detect the 1612 MHz line to a limit of 0.2 Jy, although the 1667 and 1665 MHz lines are strong. If the initial detection was valid, this may be another example of a ‘dead’ OH/IR star.

Based on studies of OH variability in very dusty OH/IR stars, it has been concluded that OH/IR stars become non-variable just before the planetary nebula stage (Olonon et al. 1984; Bedijn 1987; Van der Veen & Habing 1988). As discussed above, of our four reddest OH/IR stars, at least one is likely not an AGB star. Of the reminding three, two are clearly strongly variable in the DIRBE database. We note, however, that our sample is biased towards stars bright in the mid-infrared, thus may be somewhat prejudiced against extremely evolved objects. Olonon et al. (1984) find a turn-off of variability at about  $2.5 \log(F_{12}/F_{25})$  of  $-0.8$ . In our sample, only the LRS type A star OH 338.1 +6.4 is redder than this criteria; this star is strongly variable in the DIRBE database.

### 5.3. Carbon-Rich Stars

A similar infrared color-variability type trend is visible within the carbon-rich stars, in that carbon-rich Miras are clearly redder than carbon SRb stars. For carbon stars, increasing optical depth of the circumstellar shell, and therefore increasing redness, is expected as the star evolves (Chan & Kwok 1990). Carbon-rich Lb stars have infrared colors consistent with those of carbon-rich SRb stars. This agreement has been noted before (Kerschbaum, Lazaro, & Habison 1996).

There are too few carbon-rich SRa stars in this sample to make a conclusive statement about their infrared colors.

The carbon stars in our sample without previously known variability have colors similar to those of known Miras, suggesting that many of these objects may also be Miras, but are too optically faint to have been monitored and classified. This is confirmed by inspection of the DIRBE light curves of these objects (for example, see Figures 4G and H). Of the thirteen carbon-rich stars without variability information, twelve are clearly variable in the DIRBE light curves, and the thirteenth is probably variable. The DIRBE amplitudes of variation for these objects are large, on average 1 magnitude at  $4.9 \mu\text{m}$ , 0.6 magnitudes at  $12 \mu\text{m}$ , and 0.5 magnitudes at  $25 \mu\text{m}$ . These are slightly larger than the amplitudes of variation of the known Miras in the sample (Table 7). The three carbon stars with unspecified variability also have large amplitudes (Table 7). This implies that essentially all of the very red carbon stars in the IRAS catalog are likely previously unclassified Mira variables. For 7 of these 13 carbon-rich stars, we are able to make a rough lower limit to the pulsation period from the DIRBE database. These lower limits range from 360 to 500 days, showing, as expected, that these very red stars have long pulsation periods.

#### 5.4. Carbon-Rich vs. Oxygen-Rich Stars

Table 6 shows that, for  $F_{1.25}/F_{2.2}$  and  $F_{2.2}/F_{3.5}$ , carbon-rich stars of a particular variability type are noticeably redder than oxygen-rich stars of the same variability type. The same is true for  $F_{3.5}/F_{4.9}$ , with the exception of the SRbs, where the oxygen-rich stars are redder. At  $F_{12}/F_{25}$ , for all variability types the oxygen-rich stars are redder, while at  $F_{4.9}/F_{12}$  there is little difference in the colors of the two chemical groups. These are consistent with the results of Guglielmo et al. (1993), who found that oxygen-rich stars are redder than carbon-rich stars in  $[12] - [25]$ , but bluer in  $K - L$ . As discussed by Wallerstein & Knapp (1998), redder colors for carbon stars relative to oxygen-rich stars are expected, due to the different opacities of silicate and carbon grains. Carbon dust is more opaque at short wavelengths than silicate dust, causing carbon-rich stars to be more obscured and have higher infrared excesses for the same mass loss rates. At the shortest wavelengths, the redder  $F_{1.25}/F_{2.2}$  colors of carbon stars can be accounted for by different molecular opacities in the stellar atmospheres (Marigo, Girardi, & Chiosi 2003).

In the DIRBE dataset, the three non-supergiant OH/IR stars in our sample without known variability types are as red or redder than the carbon-rich Miras, with both groups having large inferred mass loss rates. The large mass loss rates of these two groups were discussed by Chan & Kwok (1990), who concluded that both extreme carbon stars and very red OH/IR stars are immediate planetary nebulae progenitors. This implies that there are two different evolutionary tracks for AGB stars, one for carbon-rich stars and one for oxygen-rich stars. According to current theories of stellar evolution, when stars first reach the AGB, they are all oxygen-rich; later, some become carbon-rich due to dredge-up (Iben & Renzini 1983; Chan & Kwok 1990). Only stars with main sequence masses between  $\sim 1.5 - 4 M_{\odot}$  become carbon stars; higher and lower mass stars

do not go through this phase (Groenewegen, van den Hoek, & de Jong 1995; Mouhcine & Lançon 2002). For comparison, the typical OH/IR star has a main sequence mass of  $\sim 1 M_{\odot}$ , according to Likkel (1989).

### 5.5. S Stars and Stars with Mixed Chemistry

There are only four stars in our sample with optical type S, three of which are Miras. The Mira S stars in our sample have DIRBE colors more like the oxygen-rich Miras rather the carbon-rich stars. It has been suggested (de Jong 1989) that S stars are transition objects, in the process of converting from oxygen-rich to carbon-rich. This idea is supported by the AGB evolutionary calculations of Groenewegen, van den Hoek, & de Jong (1995). The S Miras in our sample tend to have somewhat larger amplitudes of variations compared to oxygen-rich and carbon-rich Miras (Table 7), but this result may not be statistically significant, since the number of S stars is very small.

There has been quite a bit of discussion in the literature about carbon stars with oxygen-rich circumstellar shells (i.e., Little-Marenin (1986); Willems & de Jong (1988); de Jong (1989)). These stars may be transition objects, stars that have recently become carbon stars and still have relic oxygen-rich shells. Our sample does not contain any carbon-rich stars with oxygen-rich shells, however, it contains something less expected: an oxygen-rich star with a carbon-rich shell. This star, GY Cam, is classified as M6 by Lee, Gore, & Bartlett (1947) and as SR: in the GCVS. GY Cam is quite variable in the DIRBE data, with an observed amplitude of  $0.96 \pm 0.04$  magnitudes at  $4.9 \mu\text{m}$  and  $0.68 \pm 0.16$  magnitudes at  $12 \mu\text{m}$ , consistent with the Miras in the sample.

This star is not unique; a few other M stars with SiC-rich shells were identified by Skinner, Griffin, & Whitmore (1990). If these IRAS identifications and optical types are correct, then these stars present an intriguing puzzle. As the carbon stage follows the oxygen-rich stage, it is difficult to explain how a carbon-rich shell can form around an oxygen-rich star. One possibility is that they are binary or confused systems, and the shell did not originate from the observed optical star. Another possibility suggested by Skinner, Griffin, & Whitmore (1990) is that these stars have C/O ratios  $\sim 1$  (i.e., they are mis-classified S stars), which can have carbon-rich shells. Follow-up observations are needed to check the IRAS association and optical spectral type of GY Cam.

### 5.6. Massive Stars

The massive stars in the sample generally show less variation in the DIRBE database than the AGB stars (see Figures 13 – 18 and Table 7). The most variable massive star in the sample is the M3/M4II OH/IR star VY CMA, which, as discussed earlier, varies by 0.16 magnitudes at  $4.9 \mu\text{m}$ ,  $\sim 0.1$  magnitude at 12 and  $25 \mu\text{m}$ , and  $\sim 3$  magnitudes at V.

All six of the SRc stars in the sample show evidence of  $>3\sigma$  variability in the DIRBE database, with observed variations of  $\sim 0.05 - 0.1$  magnitude at  $1.25 - 4.9 \mu\text{m}$ . The highest S/N light curves in this class are those of  $\alpha$  Ori, which varies by  $0.12 \pm 0.01$  magnitudes at  $4.9 \mu\text{m}$  and  $0.10 \pm 0.01$  magnitude at  $12 \mu\text{m}$  (Figures 4O and P). The two Lc stars and the two bright giants classified as SRa or SRb are less clearly variable in the DIRBE data ( $\sim 3\sigma$ ). The two bright giants/supergiants not previously identified as variable ( $\alpha$  Car and c Pup) are not variable in the DIRBE data.

## 6. Summary

We have used the COBE database to extract near- and mid-infrared flux densities for 207 of the brightest infrared point sources in the sky, significantly expanding our earlier pilot study of 38 stars. The majority of these objects are asymptotic giant branch stars. From the DIRBE light curves, we made estimates of the infrared variability of these stars. At  $4.9 \mu\text{m}$ , 138 of the 207 sources are observed to be variable at the  $3\sigma$  level, and 106 sources at the  $5\sigma$  level. In this study, we have identified 18 variable stars not previously known to be variable.

The DIRBE colors become increasingly redder along the sequence optically-bright slightly-varying giant  $\rightarrow$  SRb  $\rightarrow$  SRa  $\rightarrow$  Mira  $\rightarrow$  OH/IR stars, with carbon stars being redder than oxygen-rich stars for the same variability type. The colors and variability of the Lb stars are consistent with those of the SRb stars, supporting previous assertions that these are the same type of object. The DIRBE variability also increases along this sequence; optically-bright giants have little to no observed variability in the DIRBE data, while the reddest stars vary by up to  $\sim 1$  magnitude at  $4.9 \mu\text{m}$  and  $\sim 0.8$  magnitudes at  $12 \mu\text{m}$ .

Table 1 and 5 are available in electronic form, from the *Astronomical Journal* electronic edition at <http://www.journals.uchicago.edu/AJ/> or at <http://www.etsu.edu/physics/bsmith/dirbe/>.

We thank the COBE team for making this project possible. We are especially grateful to Nils Odegard, for developing the software used to extract the DIRBE light curves. We also thank Danny Camper, an undergraduate at East Tennessee State University, for help with the data acquisition. We are grateful to Steve Price, Dave Leisawitz, Mark Giroux, and Don Luttermoser for helpful suggestions. This research has made use of the SIMBAD database, operated at the CDS, Strasbourg, France, as well as the Astronomical Data Center at NASA Goddard Space Flight Center, the NASA Astrophysics Data System at the Harvard-Smithsonian Center for Astrophysics, the VizieR service at the CDS, Strasbourg, France, and the Infrared Science Archive, operated by the Jet Propulsion Laboratory, California Institute of Technology. We have also made use of the electronic versions of the General Catalogue of Variable Stars, the New Suspected Variable Stars Catalogue, and the Supplement to this catalogue, provided by the Sternberg Astronomical Institute at Moscow State University. This research was funded by National Science Foundation POWRE grant AST-0073853 and NASA LTSA grant NAG5-13079.

## REFERENCES

- Anandarao, B. G., Pottasch, S. R., & Vaidya, D. B. 1993, *A&A*, 273, 570
- Baud, B., Habing, H. J., Matthews, H. E., & Winnberg, A. 1981, *A&A*, 95, 156
- Baud, B. & Habing, H. J. 1983, *A&A*, 127, 73
- Bedding, T. R., Zijlstra, A. A., Jones, A., & Foster, G. 1998, *MNRAS*, 301, 1073
- Bedijn, P. J. 1987, *A&A*, 186, 136
- Beichman, C. A., Neugebauer, G., Habing, H. J., Clegg, P. E., & Chester, T. J. 1988, Explanatory Supplement for the Infrared Astronomical Satellite Catalogs and Atlases (Washington, D.C.: US GPO)
- Bessell, M. S., & Brett, J. M. 1988, *PASP*, 100, 1134
- Boggess, N. W., et al. 1992, *ApJ*, 397, 420
- Burdick, S. V., & Murdock, T. L. 1997, ‘COBE Final Report: DIRBE Celestial Calibration’, Technical Report, General Research Corporation, Danvers MA
- Buscombe, W. 1998, 13th General Catalogue of MK Spectral Classification
- Chan, S. J., & Kwok, S. 1990, *A&A*, 237, 354
- Chen, P. S., Szczerba, R., Kwok, S., & Volk, K. 2001, *A&A*, 368, 1006
- Cohen, M., Schwartz, D. E., Chokshi, A., & Walker, R. G. 1987, *AJ*, 93, 1199
- Cohen, M. 1998, *AJ*, 115, 2092
- Cutri, R. M. 2003, Explanatory Supplement to the 2MASS All Sky Data Release
- De Laverny, P., Mennessier, M. O., Mignard, F., & Mattei, J. A. 1998, *A&A*, 330, 169
- De Jong, T. 1989, *A&A*, 223, L23
- Dickinson, D. F., Bechis, K. P., & Barrett, A. H. 1973, *ApJ*, 180, 831
- Egan, M. P., Price, S. D., Moshir, M. M., Cohen, M., & Tedesco, E. 1999, The Midcourse Space Experiment Point Source Catalog Version 1.2 Explanatory Guide, Technical Report, AD-A381933, AFRL-VS-TR-1999-1522
- Egan, M. P., & Price, S. D. 1996, *AJ*, 112, 2862
- Epchtein, N., Le Bertre, T., Lépine, J. R. D., Marques dos Santos, P., Matsuura, O. T., & Picazzio, E. 1987, *A&AS*, 71, 39

- Etoka, S., Blaszkiewicz, L., Szymczak, M., & Squeren, A. M. 2001, *A&A*, 378, 522
- Gaylard, M. J., West, M. E., Whitelock, P. A., & Cohen, R. J. 1989, 236, 247
- Gezari, D. Y., Pitts, P. S., & Schmitz, M. 1999, *Catalog of Infrared Observations*, version 5.
- Groenewegen, M. A. T., van den Hoek, L. B., & de Jong, T. 1995, *A&A*, 293, 381
- Guglielmo, F., Epchtein, N., Le Betre, T., Fouqué, P., Hron, J., Kerschbaum, F., & Lépine, J. R. D. 1993, *A&AS*, 99, 31
- Harvey, P. M., Bechis, K. P., Wilson, W. J., & Ball, J. A. 1974, *ApJS*, 27, 331
- Hauser, M. G., Kelsall, T., Leisawitz, D., & Weiland, J. 1998, ‘COBE Diffuse Infrared Background Experiment (DIRBE) Explanatory Supplement’, V. 2.3.
- Hawkins, G. W. 1989, *BAAS*, 21, 1112
- Hawkins, G. W. 1990a, ‘Extended Far-Infrared Emission from Evolved Stars and Planetary Nebulae’, Ph.D.Dissertation, U.C.L.A
- Hawkins, G. W. 1990b, *A&A*, 229, L5
- He, J. H., & Chen, P. S. 2001, *AJ*, 121, 2752
- Helou, G., & Walker, D. W. 1985, ‘IRAS Small Scale Structure Catalog’, (Pasadena: Jet Propulsion Laboratory; Joint IRAS Science Working Group)
- Heras, A. M. et al. 2002, *A&A*, 394, 539
- Huggins, P. J., & Glassgold, A. E. 1982, *AJ*, 87, 1828
- Iben, I., Jr., & Renzini, A. 1983, *ARAA*, 21, 271
- Ivezić, Ž., & Elitzur, M. 1995, *ApJ*, 445, 415
- Ivezić, Ž., & Elitzur, M. 2000, *ApJ*, 534, L93
- Ivezić, Ž., & Knapp, G. R. 2000, *Proceedings of IAU Symposium 191: AGB Stars*, A.S.P. Conference Series, V. 203, p. 124
- IRAS Point Source Catalog (1988), Version 2, Joint IRAS Science Working Group (Washington: GPO).
- Jones, T. J., Bryra, C. O., Gehrz, R. D., Harrison, J. E., Johnson, J. J., Klebe, D. I., & Lawrence, G. F. 1990, *ApJS*, 74, 785
- Jura, M. 1986, *ApJ*, 303, 327

- Jura, M., & Kleinmann, S. G. 1992, *ApJS*, 83, 329
- Kazarovets, E. V., & Durlevich, O. V. 1998, ‘New Catalogue of Suspected Variable Stars Supplement’, Version 1.0, IBVS No. 4655
- Kerschbaum, F. 1998, *A&A*, 335, L69
- Kerschbaum, F., & Hron, J. 1992, *A&A*, 263, 97
- Kerschbaum, F., & Hron, J. 1994, *A&AS*, 106, 397
- Kerschbaum, F., Lazaro, C., & Habison, P. 1996, *A&AS*, 118, 397
- Kerschbaum, F., Lebzelter, T., & Lazaro, L. 2001, *A&A*, 375, 527
- Knapp, G. R., & Morris, M. 1985, *ApJ*, 292, 640
- Kholopov, P. N. et al. 1985-1988, General Catalogue of Variable Stars
- Kukarin, B. V. et al. 1982, ‘New Catalogue of Suspected Variable Stars’, (Moscow: Publication Office ‘Nauka’)
- Kwok, S., Volk, K., & Bidelman, W. P. 1997, *ApJS*, 112, 557
- Le Bertre, T. 1992, *A&AS*, 94, 377
- Le Bertre, T. 1993, *A&AS*, 97, 729
- Lee, O. J., Gore, G. D., & Bartlett, T. J. 1947, Dearborn Observatory Annals
- Lewis, B. M., Eder, J., & Terzian, Y. 1990, *ApJ*, 362, 634
- Lewis, B. M. 2002, *ApJ*, 576, 445
- Likkell, L. 1989, *ApJ*, 344, 350
- Little-Marenin, I. R. & Stencel, R. E. 1992, *PASPC*, 26, 591
- Little-Marenin, I. R. 1986, *ApJ*, 307, L15
- Little-Marenin, I. R., Stencel, R. E., & Staley, S. B. 1996, *ApJ*, 467, 806
- Lockwood, G. W. & Wing, R. F. 1971, *ApJ*, 169, 63
- Marengo, M., Ivezić, Ž., & Knapp, G. R. 2001, *MNRAS*, 324, 1117
- Marigo, P., Girardi, L., & Chiosi, C. 2003, *A&A*, in press
- Mouhcine, M., & Lançon, A. 2002, *A&A*, 393, 149

- Olmon, F. M., Baud, B., Habing, H. J., de Jong, T., Harris, S., & Pottasch, S. R. 1984, *ApJ*, 278, L41
- Price, S. D., et al. 1999, ‘Astrophysics with Infrared Surveys: A Prelude to SIRTf’, *ASP Conference Series*, V. 177, 394
- Sedlmayr, E. 1994, in *Molecules in the Stellar Environment*, IAU Colloquium 146, (Springer-Verlag: New York), 163
- Skinner, C. J., Griffin, I., & Whitmore, B. 1990, *MNRAS*, 243, 78
- Sloan, G. C., & Price, S. D. 1998, *ApJS*, 119, 141
- Sloan, G. C., Little-Marenin, I. R., & Price, S. D. 1998, *AJ*, 115, 809
- Smith, B. J., Leisawitz, D., Castelaz, M. W., & Luttermoser, D. 2002, *AJ*, 123, 948
- Thronson, H. A., Jr., Latter, W. B., Black, J. H., Bally, J., & Hacking, P. 1987, *ApJ*, 322, 770
- Van der Veen, W. E. C. J., & Habing, H. J. 1988, *A&A*, 194, 125
- Van der Veen, W. E. C. J. 1989, *A&A*, 210, 127
- Volk, K., & Cohen, M. 1989, *AJ*, 98, 931
- Volk, K., & Kwok, S. 1988, *ApJ*, 331, 435
- Wallerstein, G., & Knapp, G. R. 1998, *ARAA*, 36, 369
- Wenger, M., et al. 1996, *BAAS*, 189, 602
- Willems, F. J. & de Jong, T. 1986, *ApJ*, 309, L39
- Willems, F. J., & de Jong, T. 1988, *A&A*, 196, 173
- Wolf, N. J., & Ney, E. P. 1969, *ApJ*, 155, L181
- Young, K., Phillips, T. G., & Knapp, G. R. 1993a, *ApJS*, 86, 517
- Young, K., Phillips, T. G., & Knapp, G. R. 1993b, *ApJ*, 409, 725



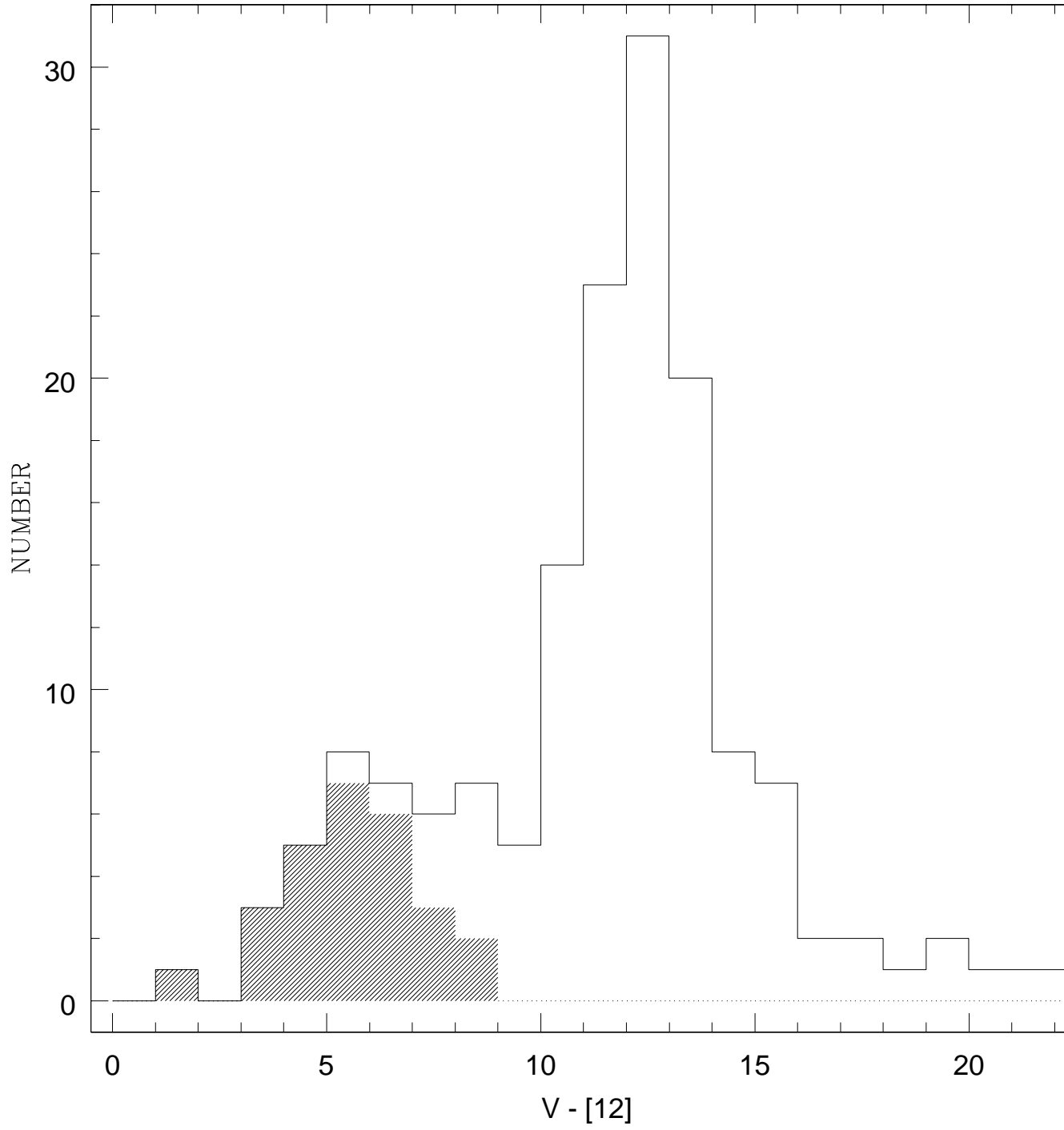
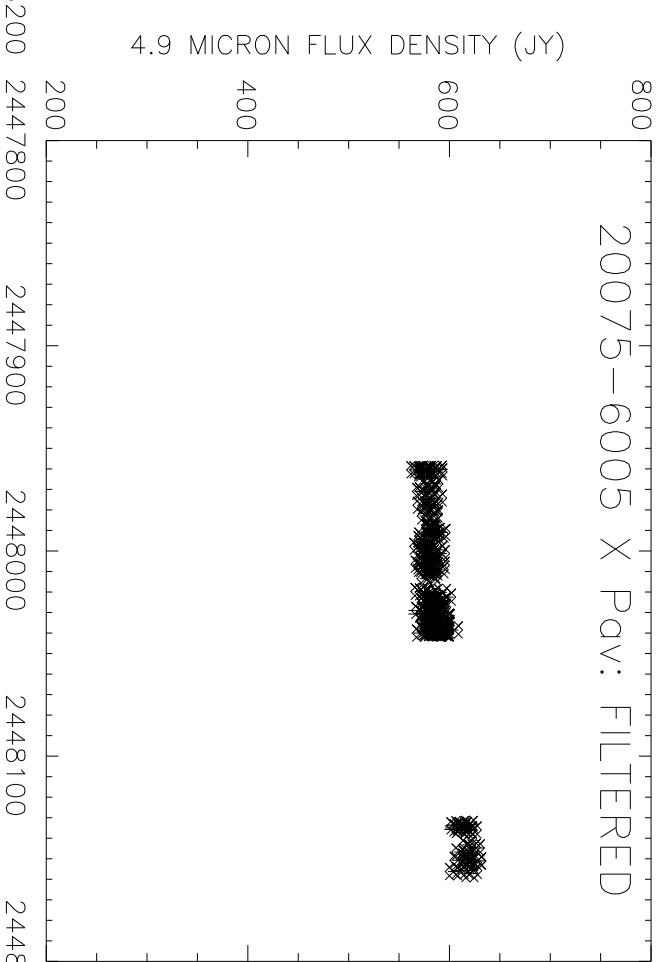
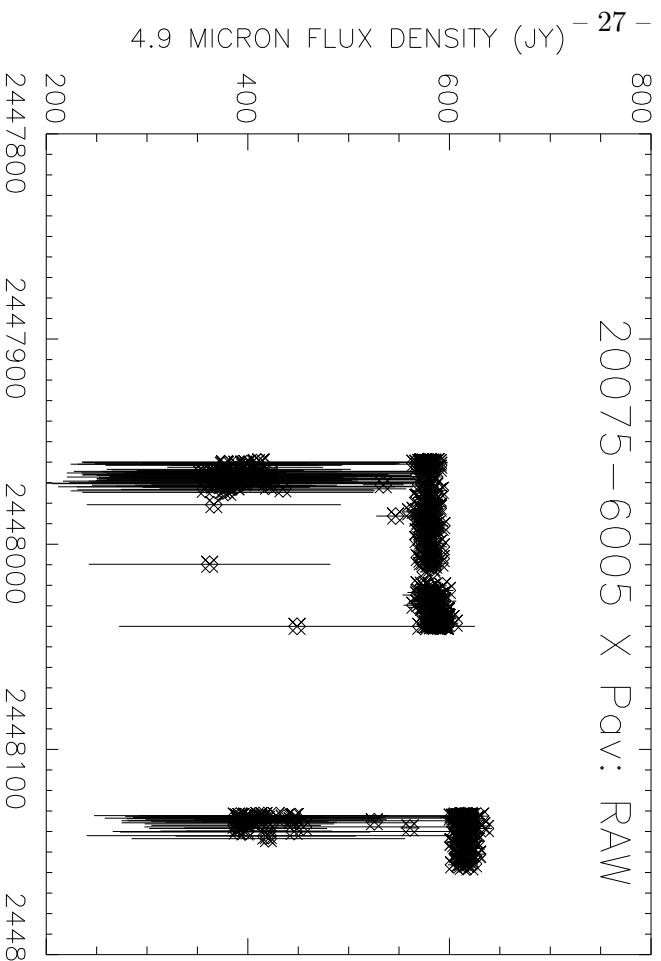
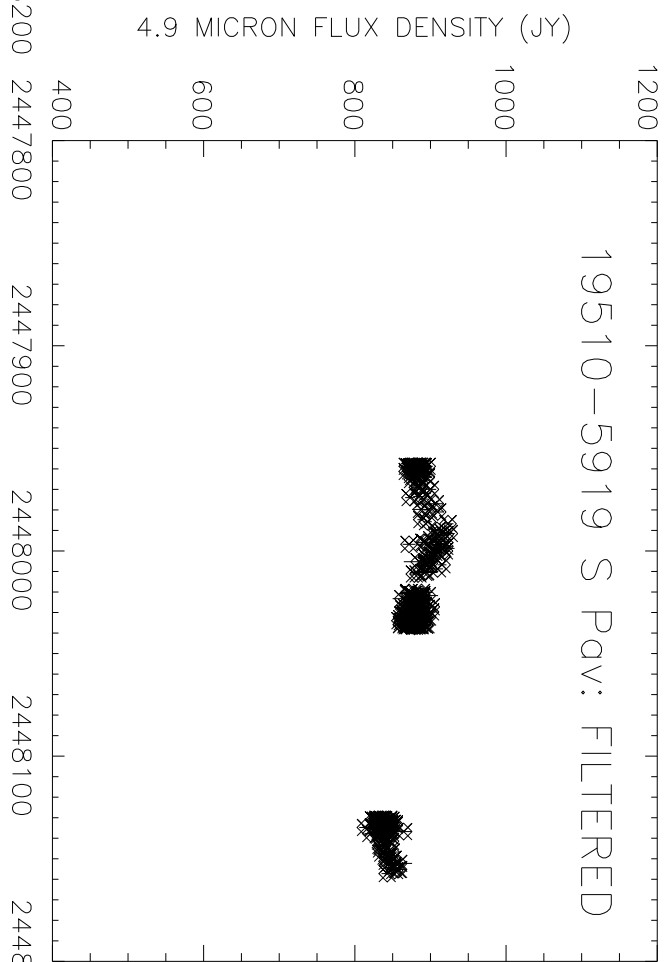


Fig. 1.— The distribution of  $V - [12]$  for the 155 sources in our sample with  $V$  magnitudes available.

The  $12\ \mu\text{m}$  magnitudes were calculated from the IRAS Point Source Catalogue  $12\ \mu\text{m}$  flux densities assuming zero magnitude corresponds to  $28.3\ \text{Jy}$  (Beichman et al. 1988). The shaded region marks the 27 stars with IRAS LRS spectral type of ‘S’ (dominated by photospheric emission). The bluest star is the F0 II star  $\alpha\ \text{Car}$  (Canopus). Note that this histogram is likely incomplete at  $V - [12] > 11.8$ , which corresponds to a  $V = 10$  magnitude star at our  $12\ \mu\text{m}$  flux limit.



JULIAN DAY - 2440000

Fig. 2.— Examples of raw vs. filtered  $4.9 \mu\text{m}$  DIRBE light curves for a few selected objects, the SRa star S Pav and the SRb star X Pav. The filtering process is described in the text.

Fig. 3.— Some representative filtered light curves. See text for more details.

Fig. 4.— Some more representative filtered light curves. See text for more details.

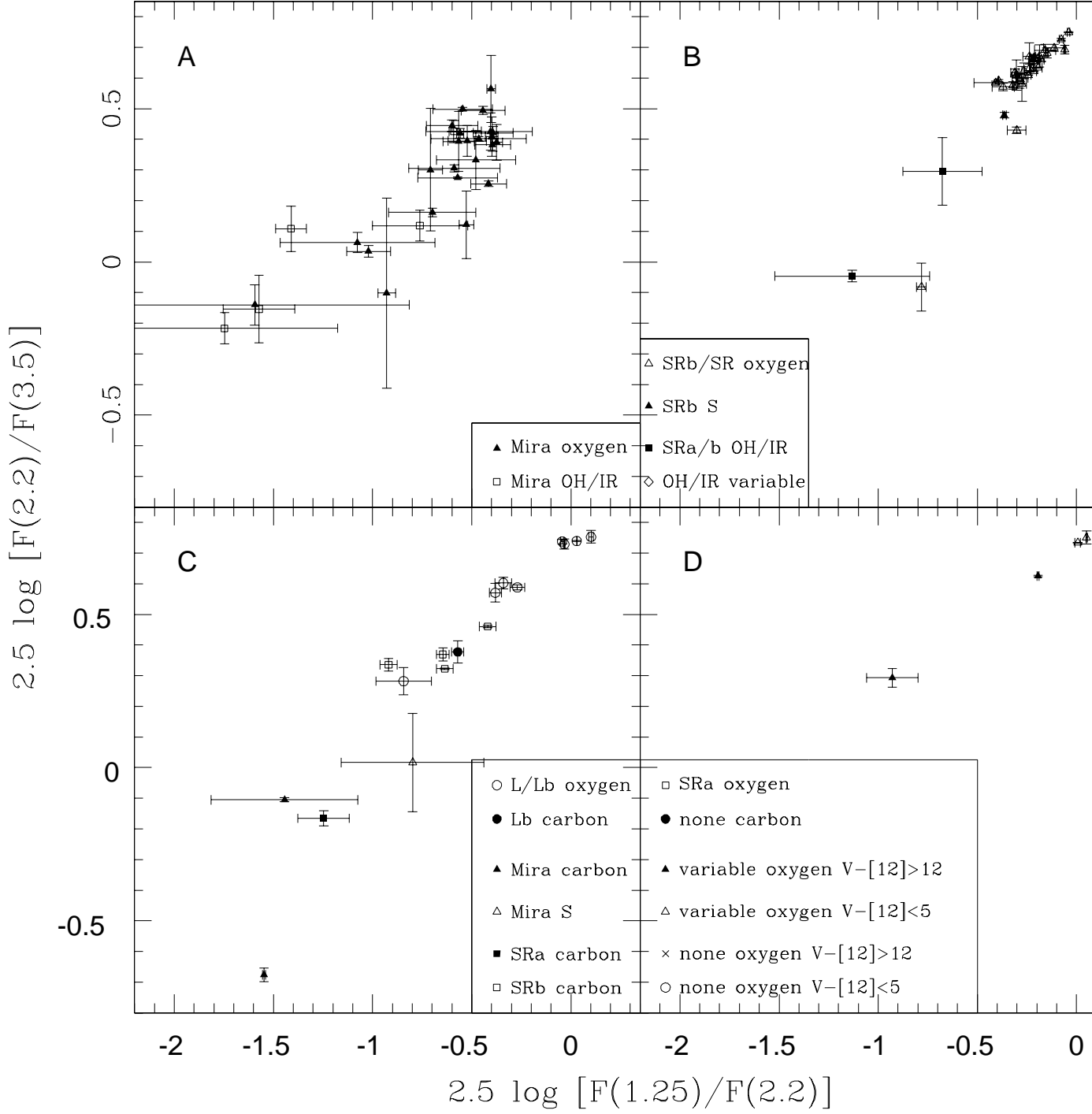


Fig. 5.— The time-averaged DIRBE 2.2  $\mu\text{m}/3.5 \mu\text{m}$  vs. 1.25  $\mu\text{m}/2.2 \mu\text{m}$  color-color plot, for

types of stars associated with the AGB. For clarity, four panels with different types of objects are shown. The symbols corresponding to different types of stars are as shown (‘none’ refers to stars not previously identified as variable.) The errorbars shown are the standard deviations of the observed infrared colors of the stars, and therefore include both intrinsic color variations and measurement uncertainties. This plot only includes stars with average  $S/N > 5$  at all three wavelengths.

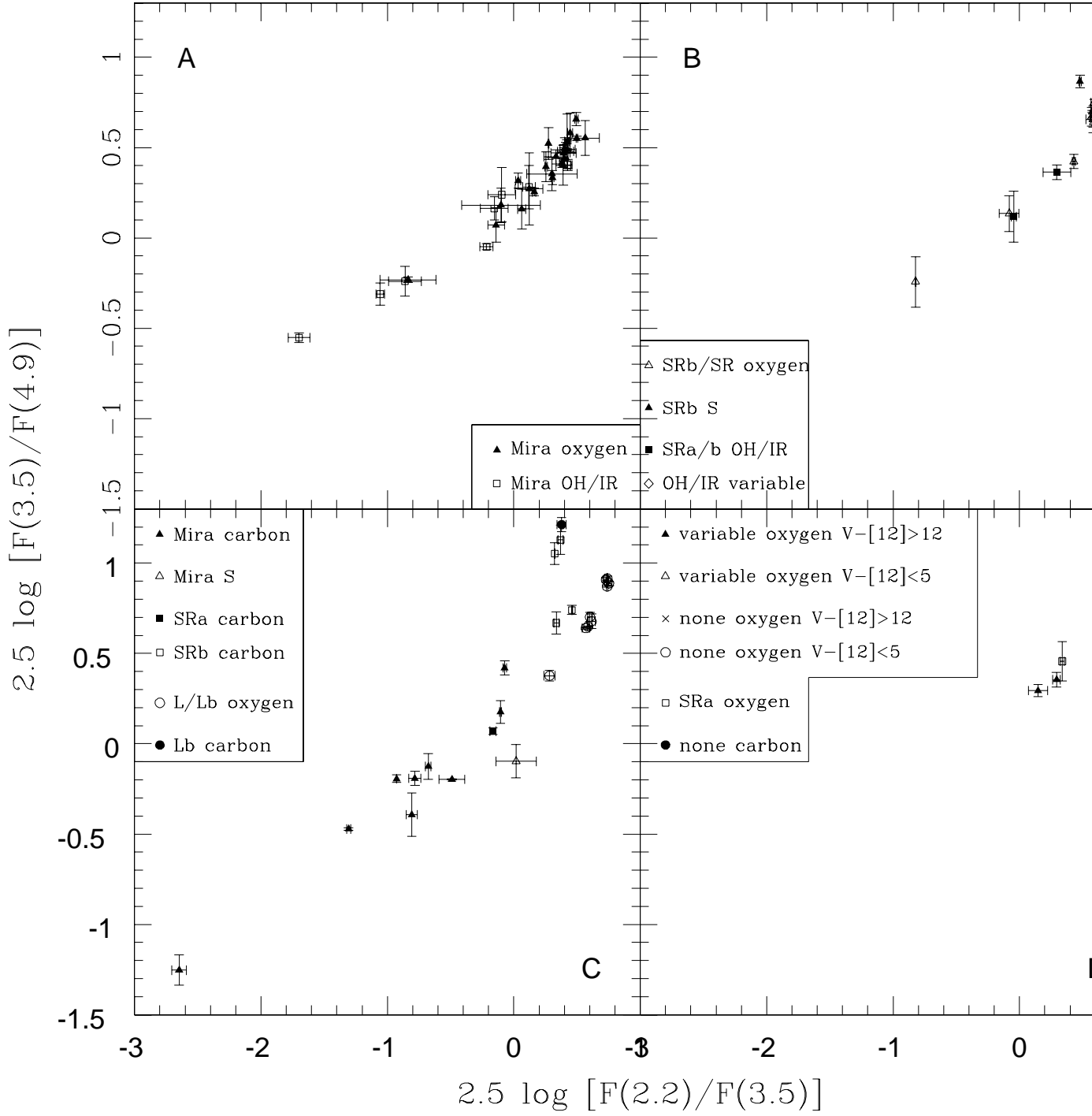


Fig. 6.— The time-averaged DIRBE  $3.5 \mu\text{m}/4.9 \mu\text{m}$  vs.  $2.2 \mu\text{m}/3.5 \mu\text{m}$  color-color plot. The sym-

bols are as shown. The errorbars shown are the standard deviations of the observed infrared colors of the stars, and therefore include both intrinsic color variations and measurement uncertainties. This plot only includes stars with average  $S/N > 5$  at all three wavelengths.



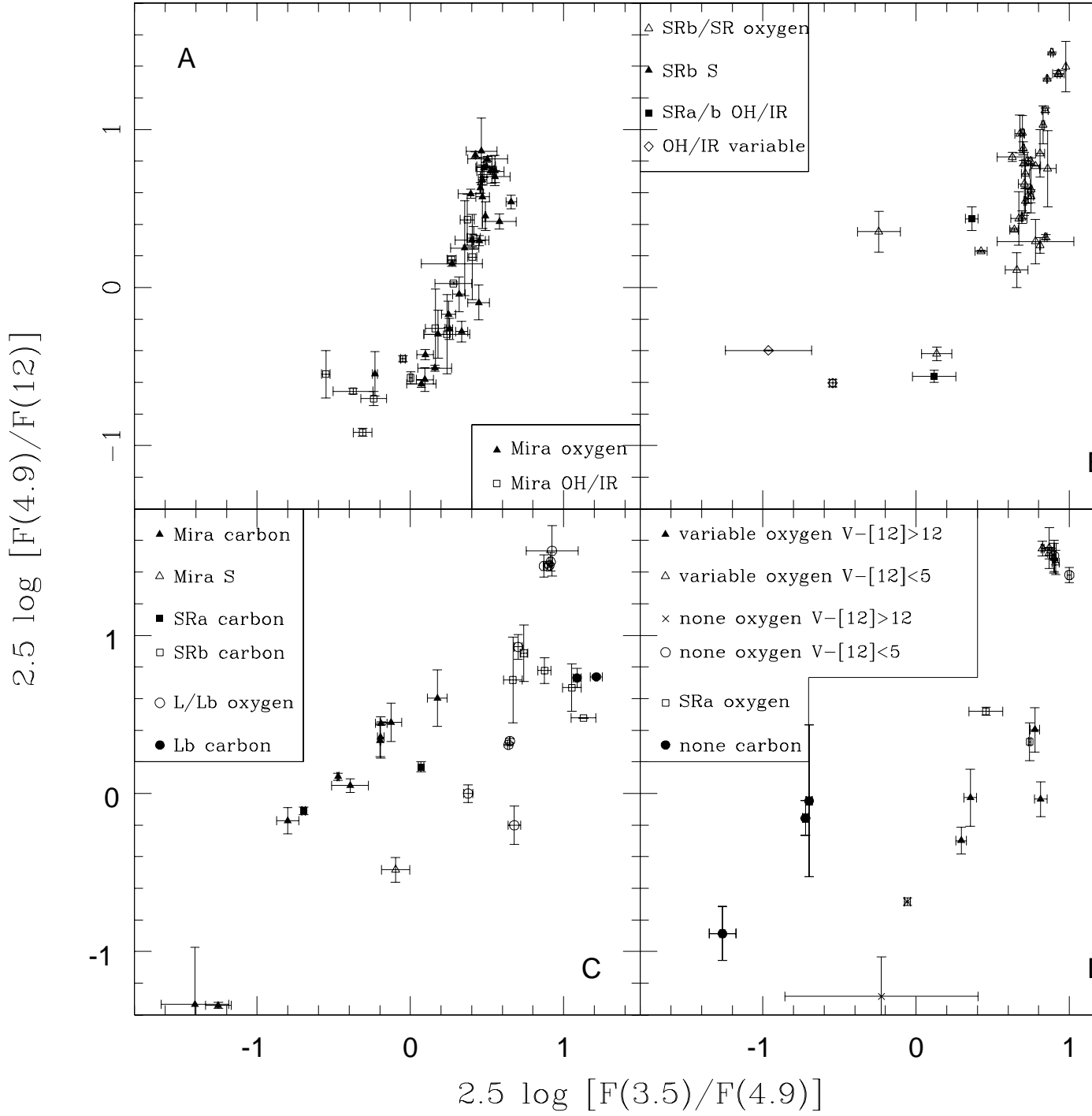


Fig. 7.— The time-averaged DIRBE 4.9  $\mu\text{m}/12 \mu\text{m}$  vs. 3.5  $\mu\text{m}/4.9 \mu\text{m}$  color-color plot. The

symbols are as shown. The errorbars shown are the standard deviations of the individual flux measurements, and therefore include both intrinsic variations of the sources as well as measurement uncertainties. This plot only includes stars with average  $S/N > 5$  at all three wavelengths.

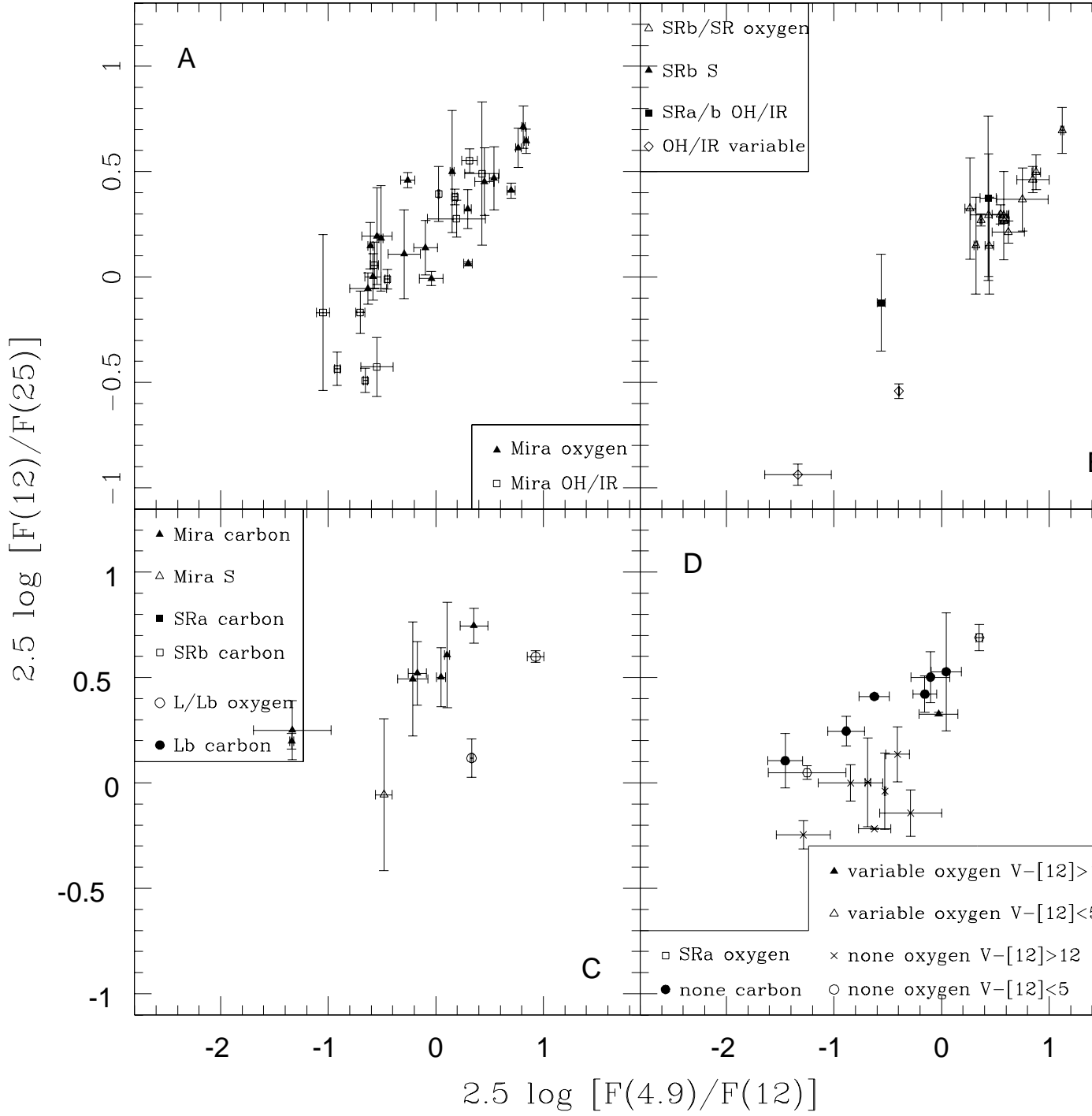


Fig. 8.— The time-averaged DIRBE 12  $\mu\text{m}/25 \mu\text{m}$  vs. 4.9  $\mu\text{m}/12 \mu\text{m}$  color-color plot. The symbols

are as shown. The errorbars shown are the standard deviations of the infrared colors and therefore include both intrinsic color variations and measurement uncertainties.

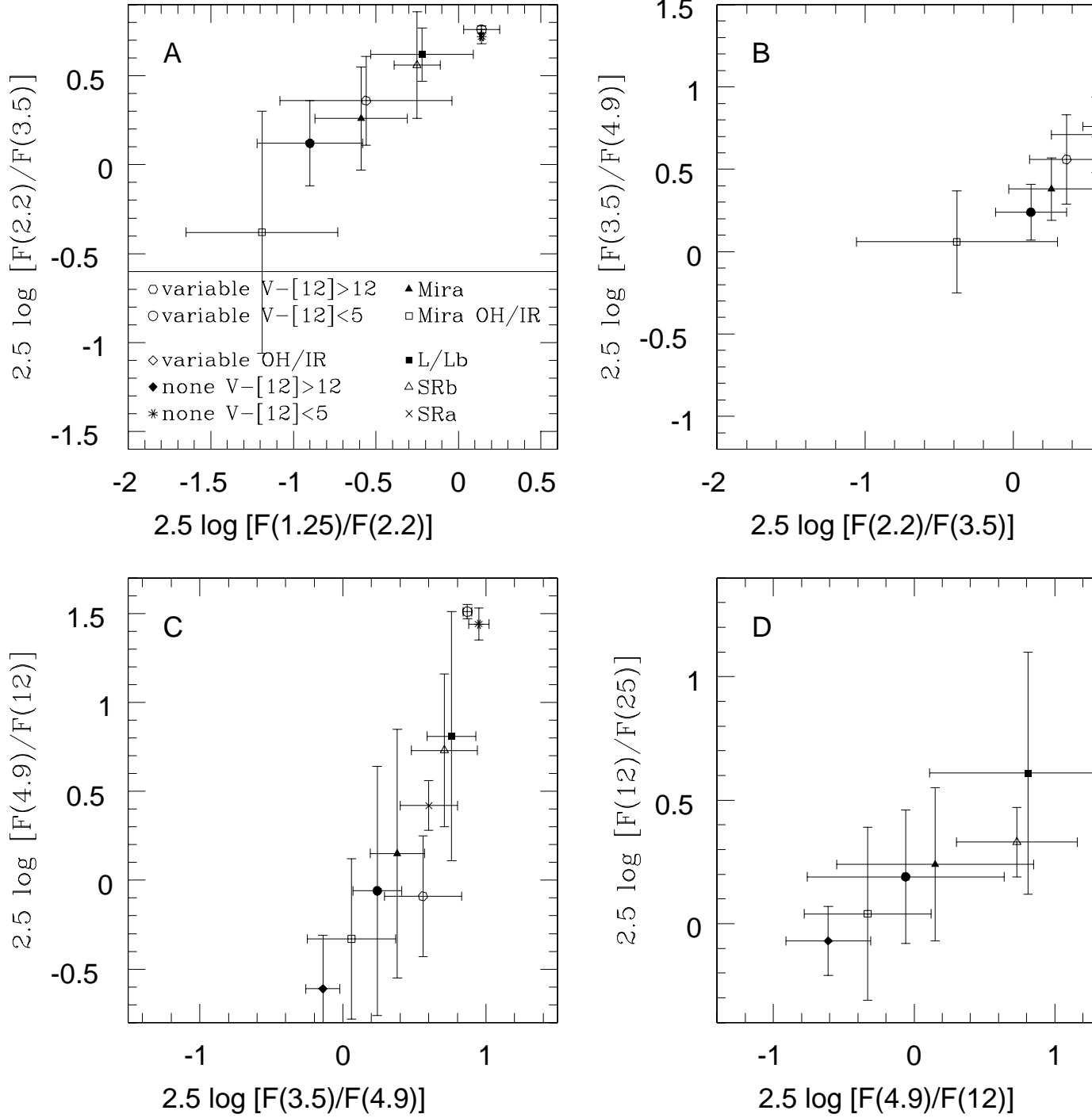


Fig. 9.— This Figure shows the means of the time-averaged DIRBE colors for different types of

oxygen-rich stars associated with the AGB, along with the rms spread (from Table 6). The symbols identified in panel A correspond to datapoints in all four panels. Categories with less than two high quality measurements at all three wavelengths are not shown.

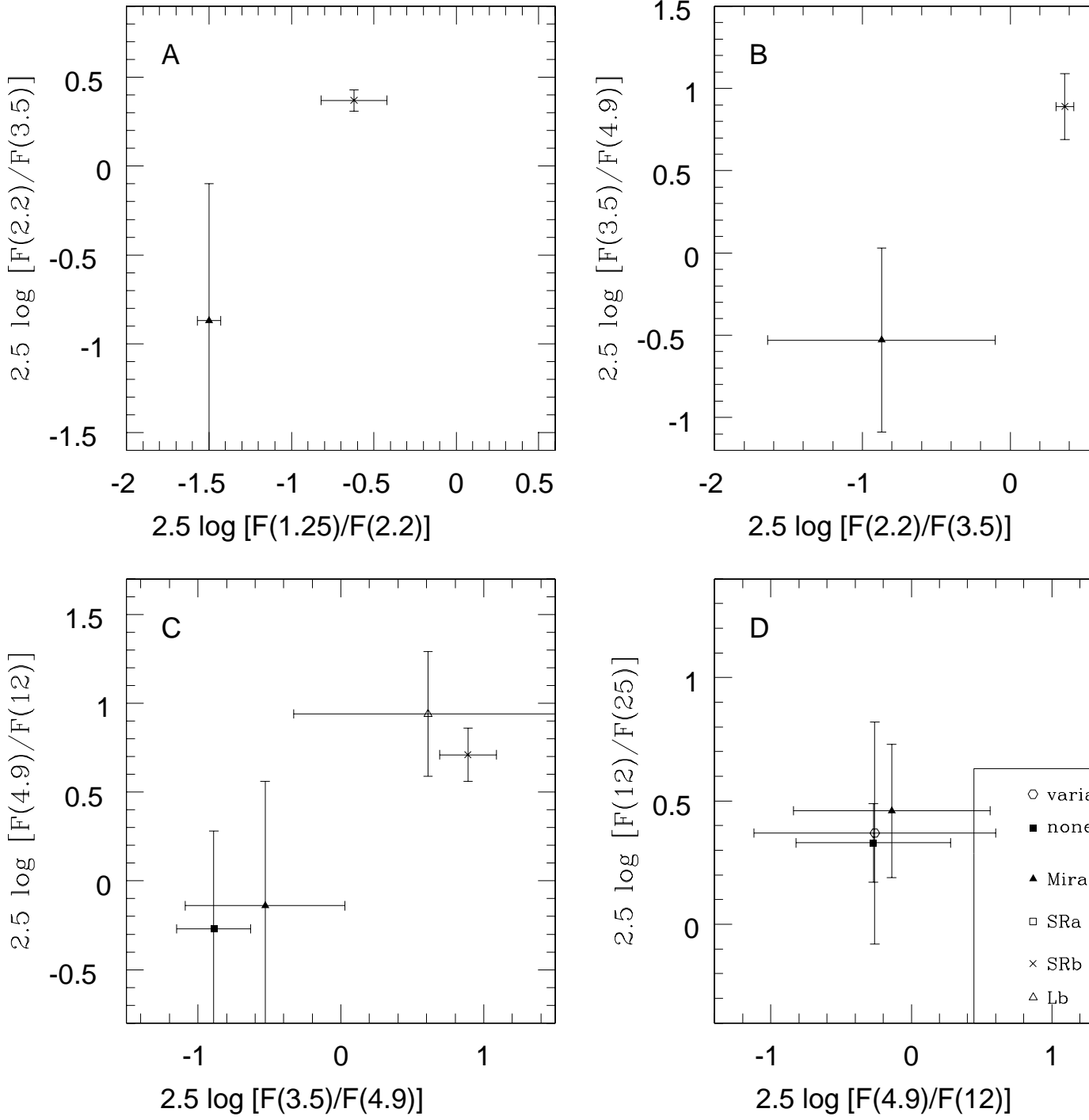


Fig. 10.— This Figure shows the mean of the time-averaged DIRBE colors for the different types of

carbon-rich stars in the sample, along with the rms spread (from Table 6). The symbols identified in panel D correspond to datapoints in all four panels. Categories with less than two high quality measurements at all three wavelengths are not shown. In Panel B, two datapoints are superposed (the means for the unspecified variables and the stars not previously known to be variable are the same).



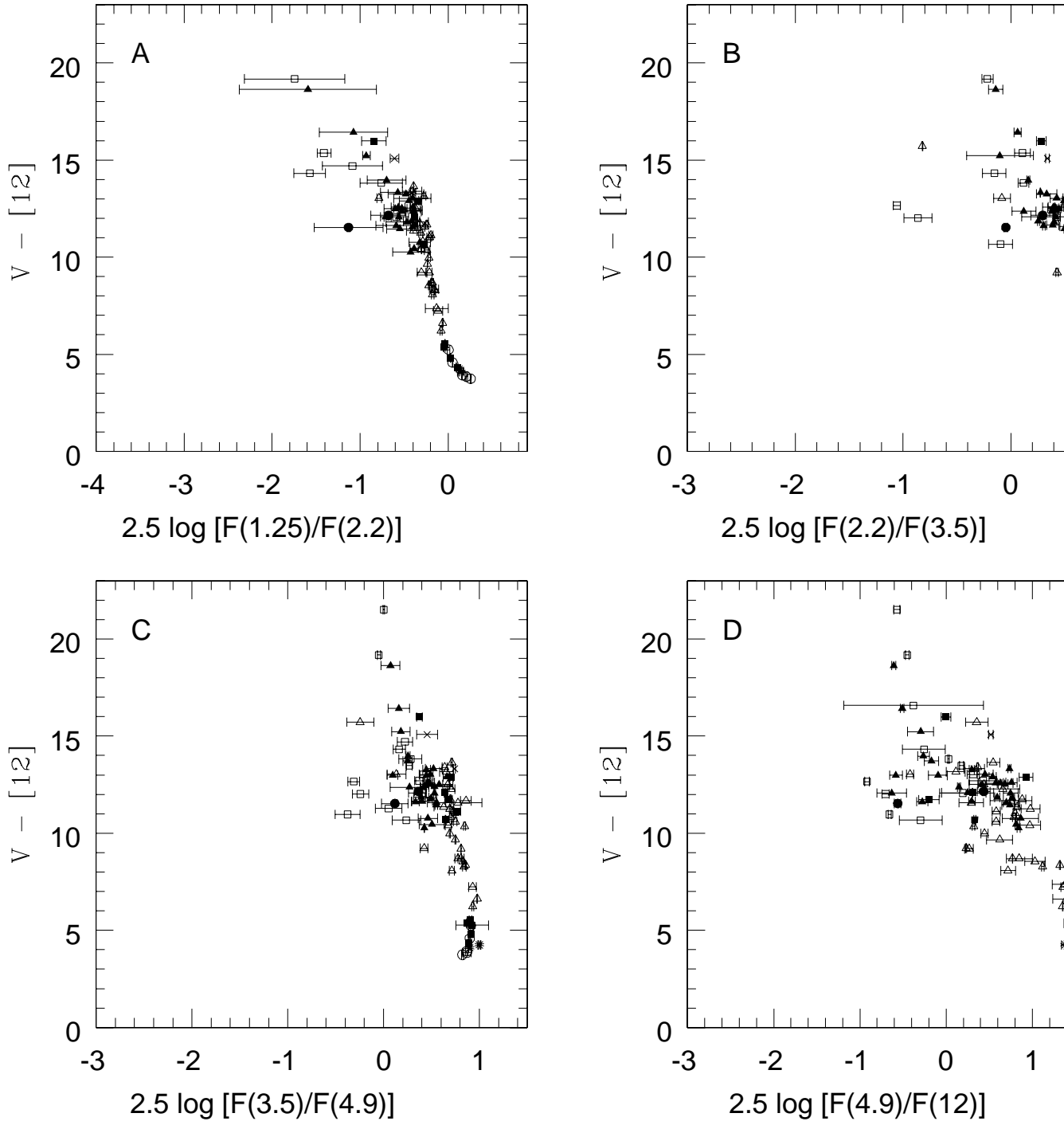


Fig. 11.— This Figure shows the mean DIRBE colors for the different types of oxygen-rich stars

associated with the AGB, plotted against  $V - [12]$ . The symbols are as in Figure 9.

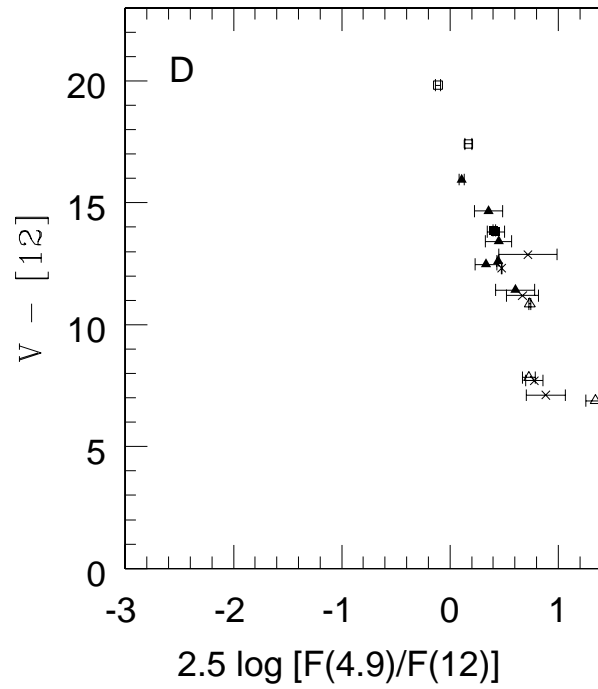
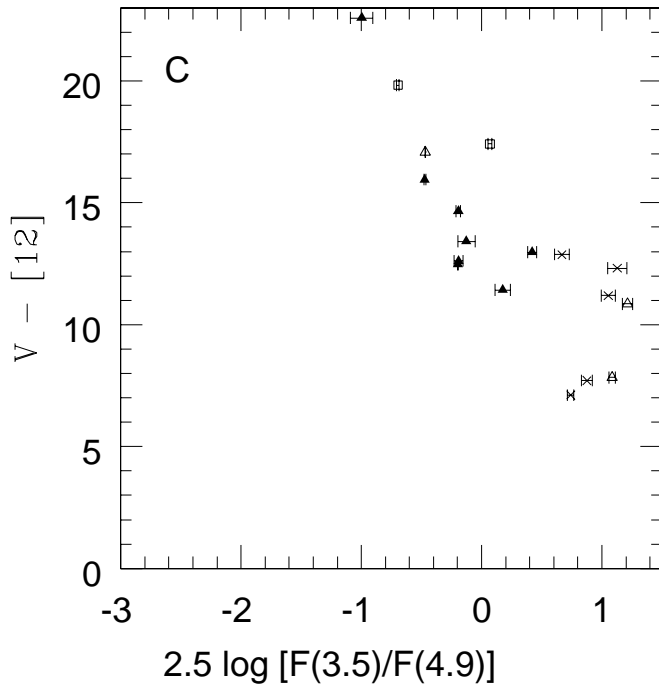
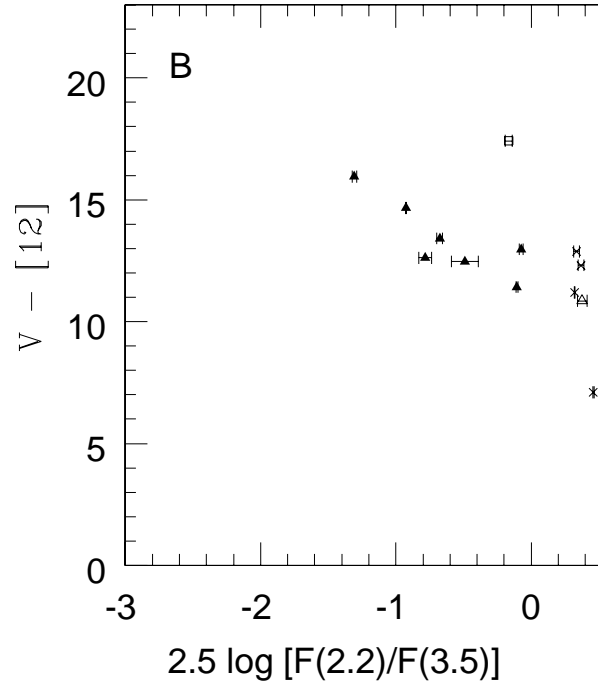
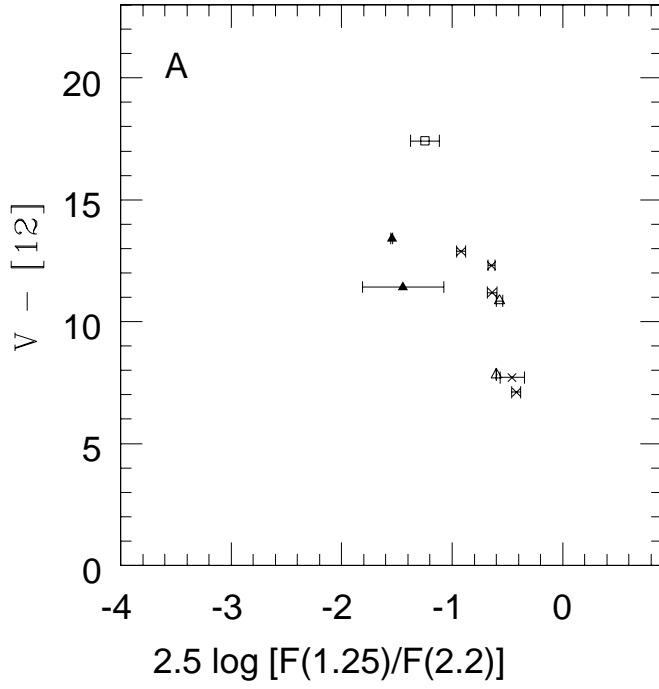


Fig. 12.— This Figure shows the mean DIRBE colors for the different types of carbon-rich stars associated with the AGB, plotted against  $V - [12]$ . The symbols are as in Figure 10. The SRa (open square) at  $V - [12] = 19.8$  is RW LMi; the SRa at  $V - [12] = 19.8$  is V Hya. The very red Mira (filled triangle) at  $V - [12] = 22.6$  is LP And.

1.25 MICRONS

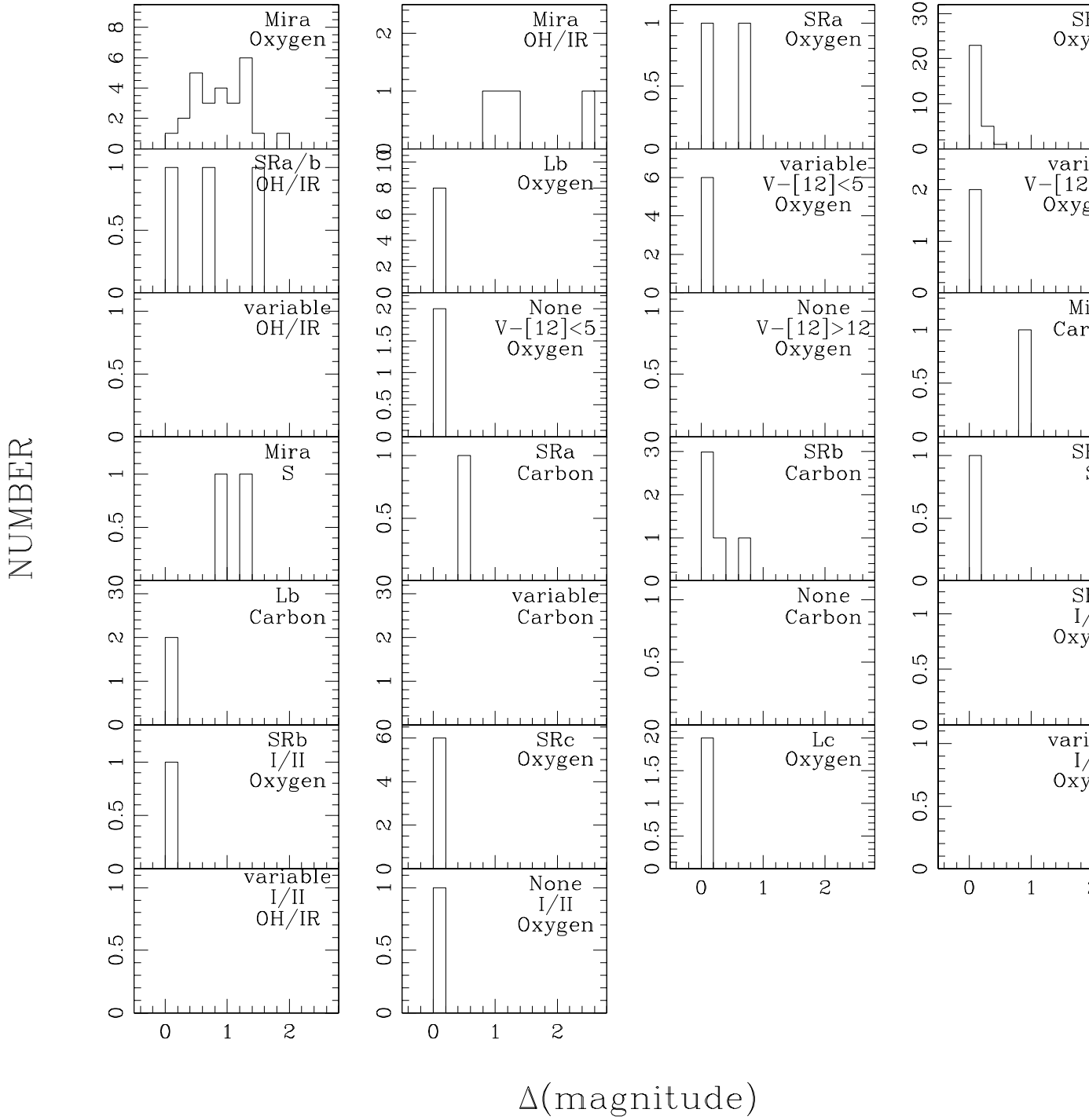


Fig. 13.— Histograms of the *observed* 1.25  $\mu\text{m}$  amplitudes of variation in the light curves of various

types of stars in our sample. Note that these amplitudes are not necessarily the full amplitude of variation for the stars, since the DIRBE data may not cover the full pulsation period. These plots only include stars with at least  $5\sigma$  DIRBE flux densities at  $1.25\ \mu\text{m}$  at minimum light. If a panel does not have a histogram, it means no star in that group was detected above  $5\sigma$  at  $1.25\ \mu\text{m}$ . The average uncertainty in the observed  $\Delta(\text{mag})$  at  $1.25\ \mu\text{m}$  for the sample is 0.06 magnitudes.

2.2 MICRONS

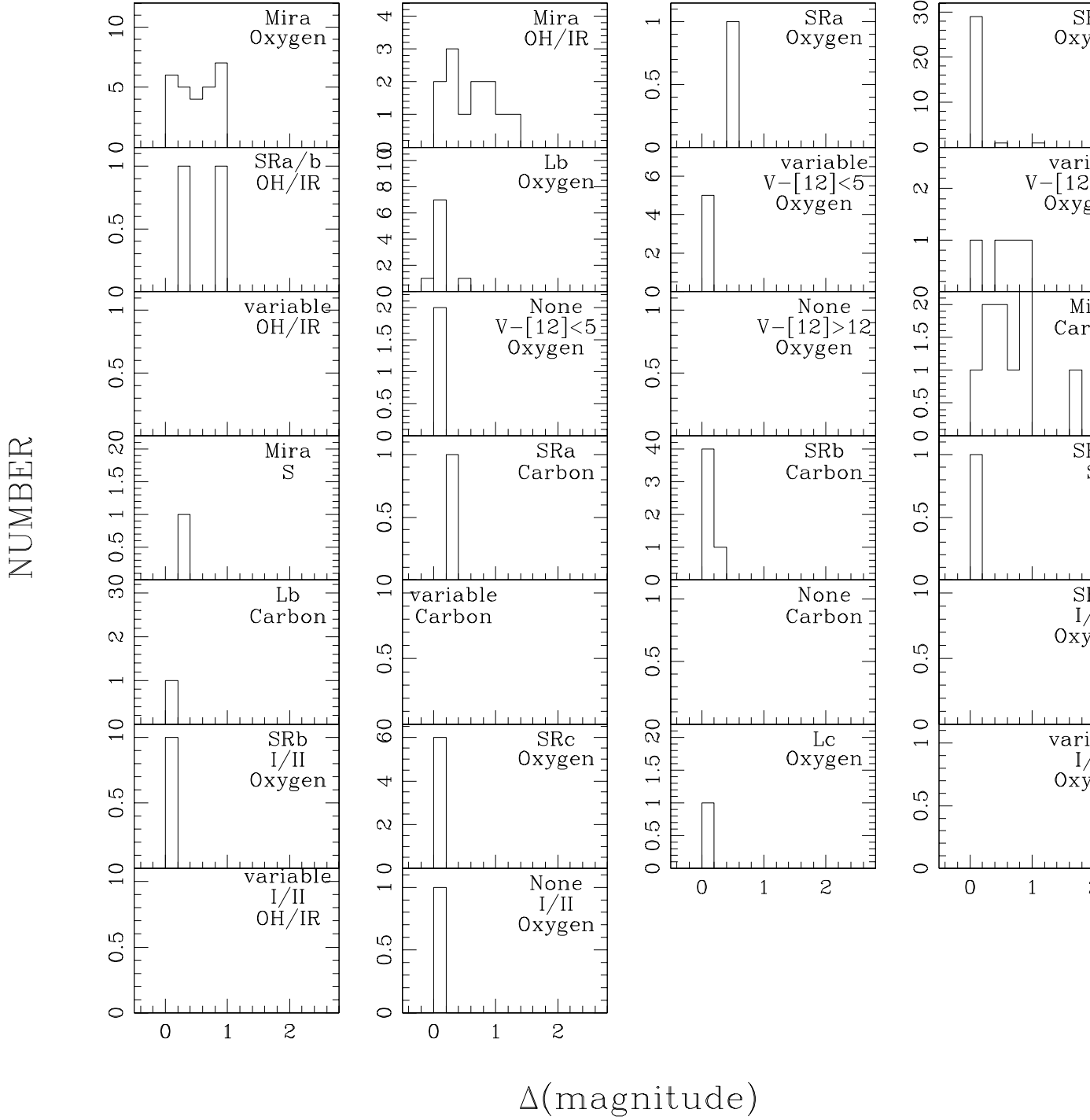


Fig. 14.— Histograms of the *observed* 2.2 μm amplitudes of variation in the light curves of various

types of stars in our sample. Note that these amplitudes are not necessarily the full amplitude of variation for the stars, since the DIRBE data may not cover the full pulsation period. These plots only include stars with at least  $5\sigma$  DIRBE flux densities at  $2.2 \mu\text{m}$  at minimum light. If a panel does not have a histogram, it means no star in that group was detected above  $5\sigma$  at  $2.2 \mu\text{m}$ . The average uncertainty in the observed  $\Delta(\text{mag})$  at  $2.2 \mu\text{m}$  for the sample is 0.05 magnitudes.

### 3.5 MICRONS

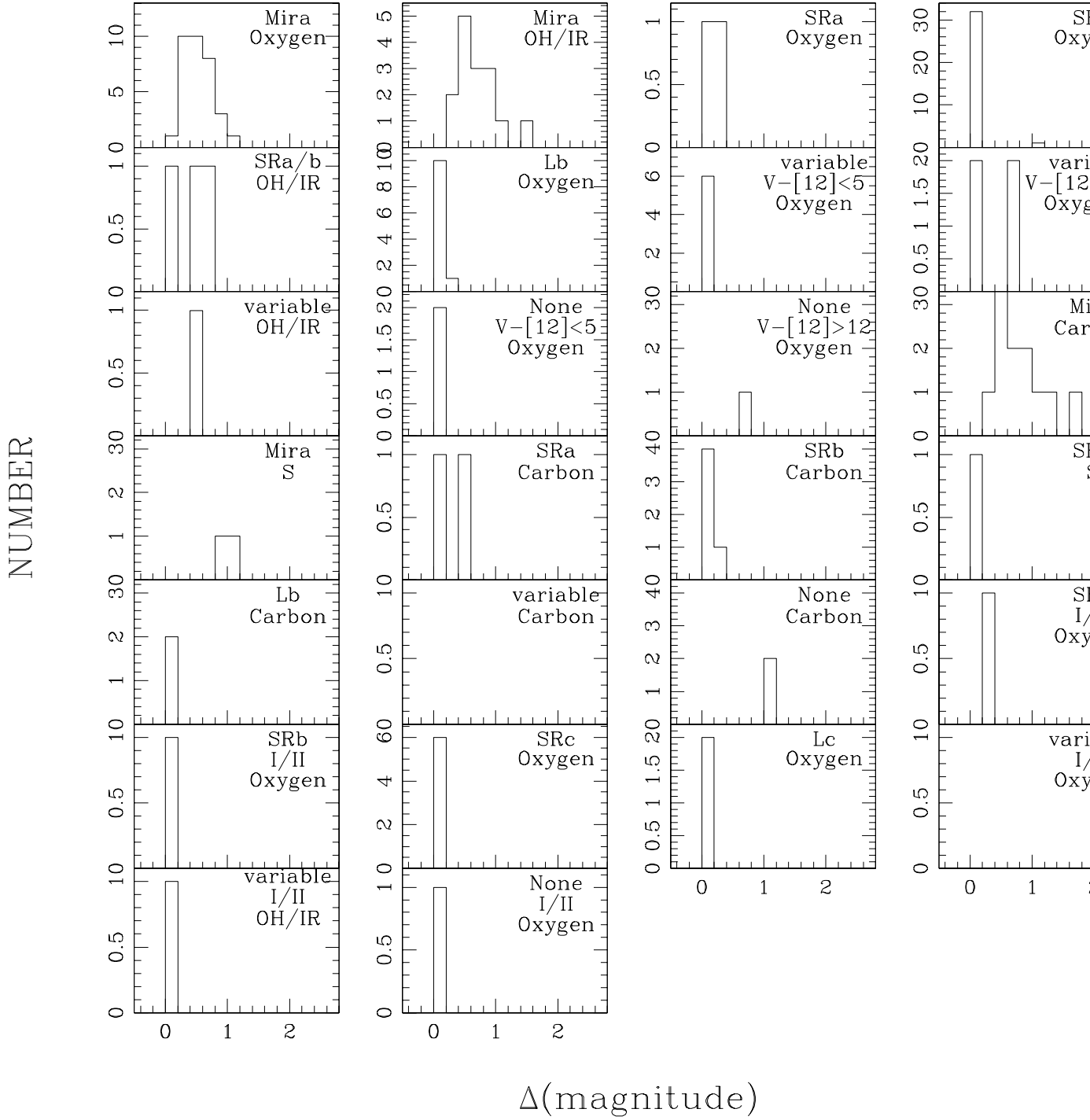


Fig. 15.— Histograms of the *observed* 3.5 μm amplitudes of variation in the light curves of various



types of stars in our sample. Note that these amplitudes are not necessarily the full amplitude of variation for the stars, since the DIRBE data may not cover the full pulsation period. These plots only include stars with at least  $5\sigma$  DIRBE flux densities at  $3.5 \mu\text{m}$  at minimum light. If a panel does not have a histogram, it means no star in that group was detected above  $5\sigma$  at  $3.5 \mu\text{m}$ . The average uncertainty in the observed  $\Delta(\text{mag})$  at  $3.5 \mu\text{m}$  for the sample is 0.06 magnitudes.

4.9 MICRONS

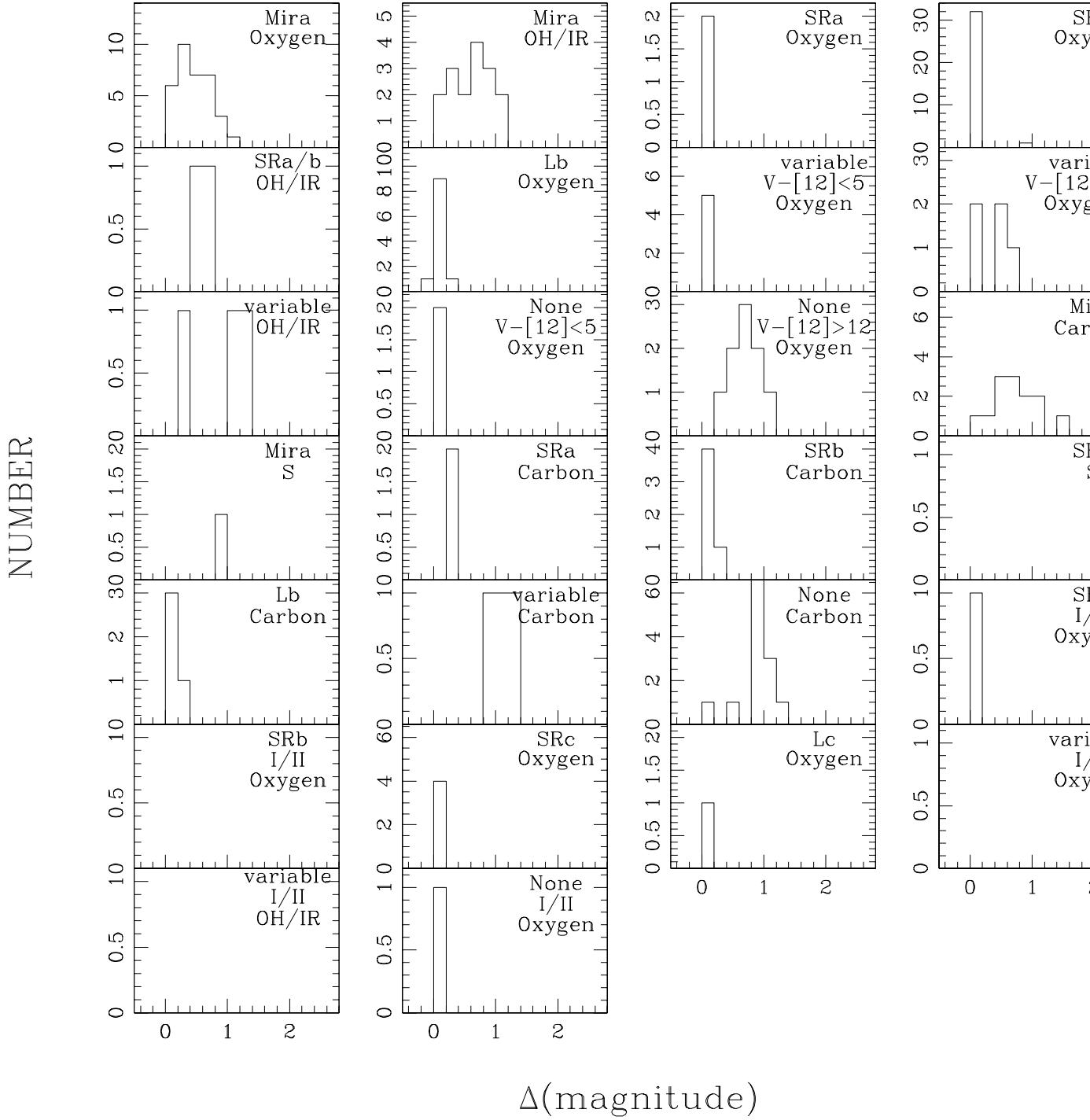


Fig. 16.— Histograms of the *observed* 4.9 μm amplitudes of variation in the light curves of various

types of stars in our sample. Note that these amplitudes are not necessarily the full amplitude of variation for the stars, since the DIRBE data may not cover the full pulsation period. These plots only include stars with at least  $5\sigma$  DIRBE flux densities at  $4.9 \mu\text{m}$  at minimum light. If a panel does not have a histogram, it means no star in that group was detected above  $5\sigma$  at  $4.9 \mu\text{m}$ . The average uncertainty in the observed  $\Delta(\text{mag})$  at  $4.9 \mu\text{m}$  for the sample is 0.05 magnitudes.

### 12 MICRONS

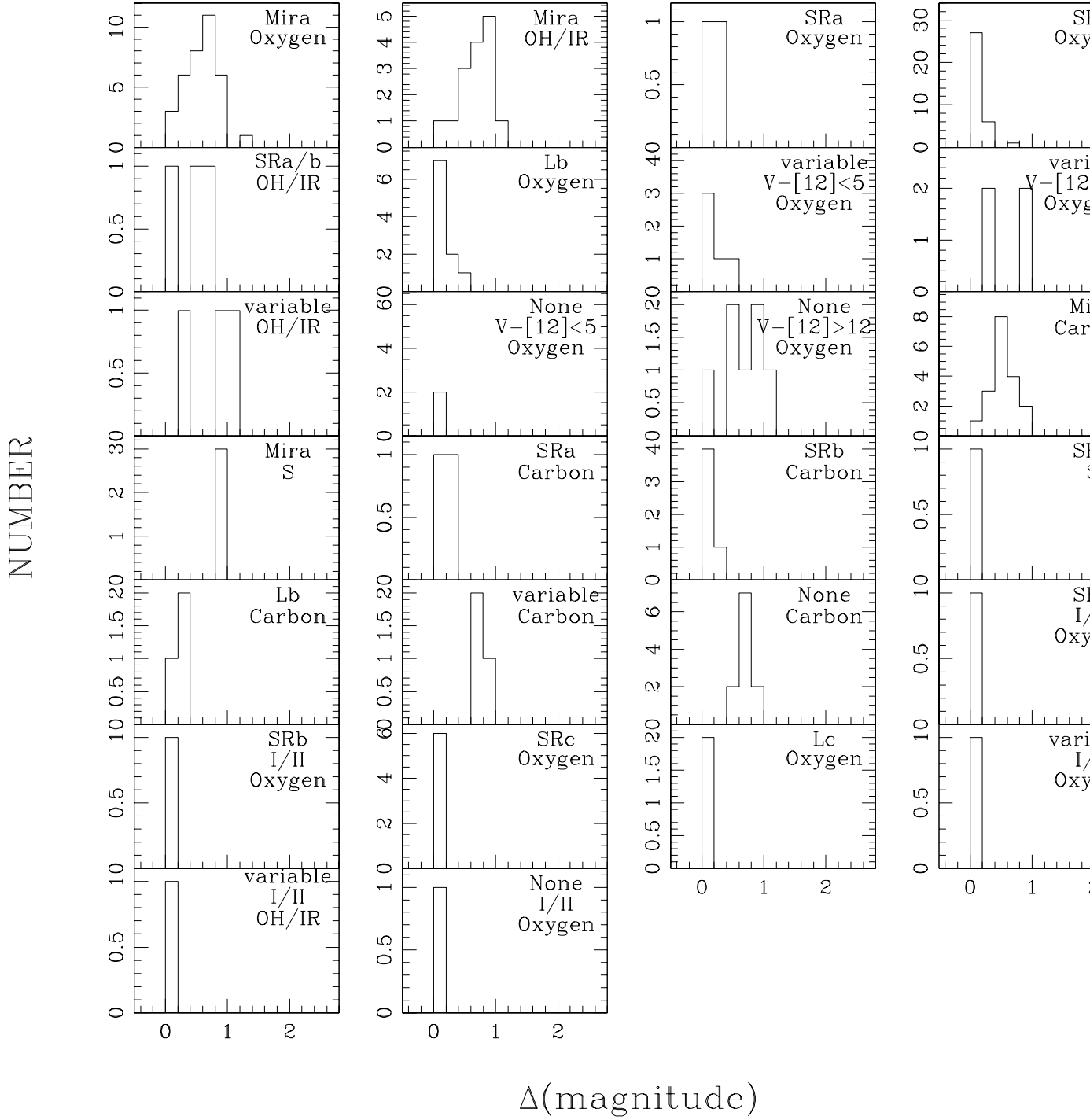


Fig. 17.— Histograms of the *observed* 12 μm amplitudes of variation in the light curves of various

types of stars in our sample. Note that these amplitudes are not necessarily the full amplitude of variation for the stars, since the DIRBE data may not cover the full pulsation period. These plots only include stars with at least  $5\sigma$  DIRBE flux densities at  $12\ \mu\text{m}$  at minimum light. If a panel does not have a histogram, it means no star in that group was detected above  $5\sigma$  at  $12\ \mu\text{m}$ . The average uncertainty in the observed  $\Delta(\text{mag})$  at  $12\ \mu\text{m}$  for the sample is 0.11 magnitudes.

### 25 MICRONS

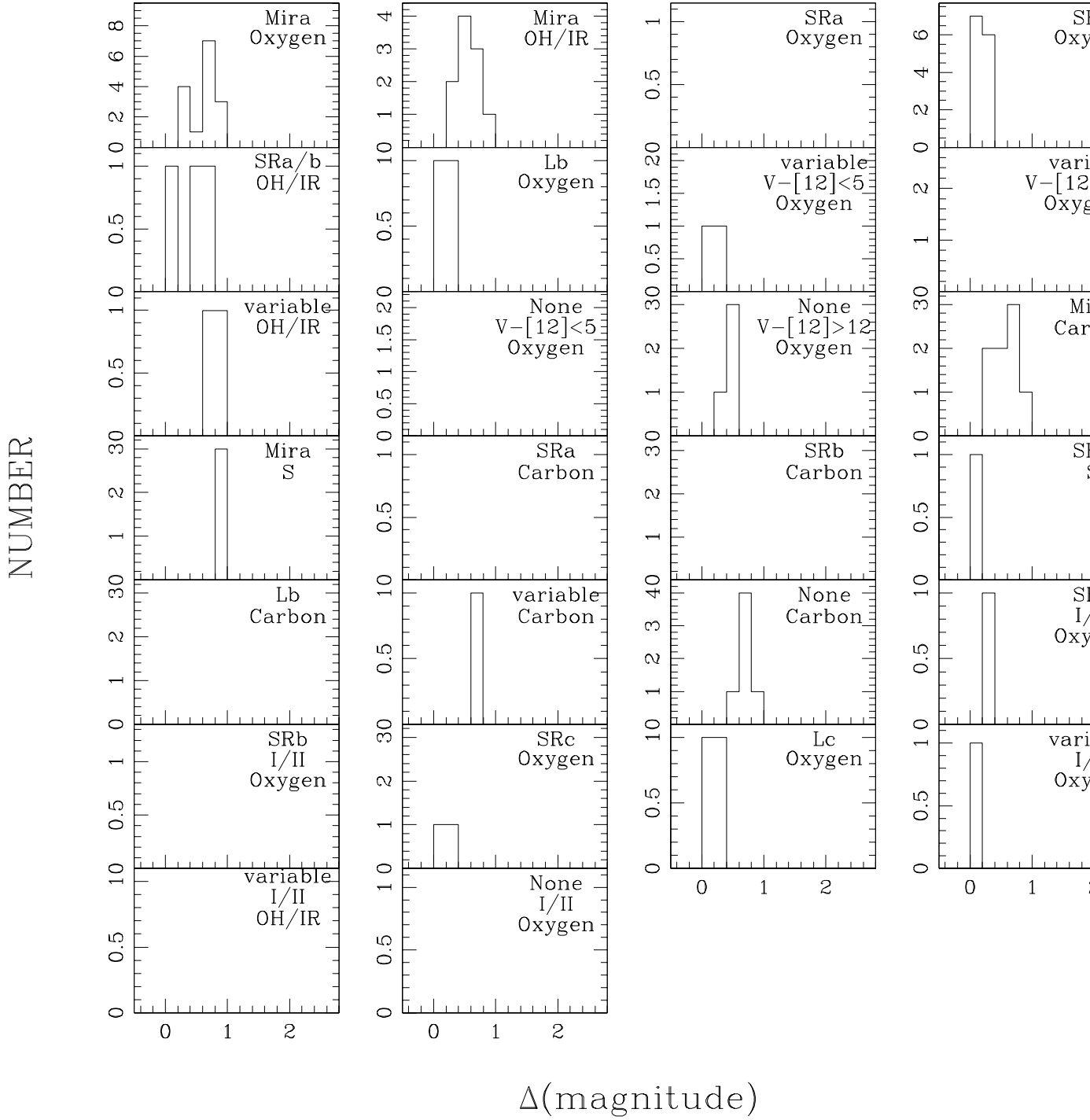


Fig. 18.— Histograms of the *observed* 25 μm amplitudes of variation in the light curves of various

types of stars in our sample. Note that these amplitudes are not necessarily the full amplitude of variation for the stars, since the DIRBE data may not cover the full pulsation period. These plots only include stars with at least  $5\sigma$  DIRBE flux densities at  $25\ \mu\text{m}$  at minimum light. If a panel does not have a histogram, it means no star in that group was detected above  $5\sigma$  at  $25\ \mu\text{m}$ . The average uncertainty in the observed  $\Delta(\text{mag})$  at  $25\ \mu\text{m}$  for the sample is 0.14 magnitudes.

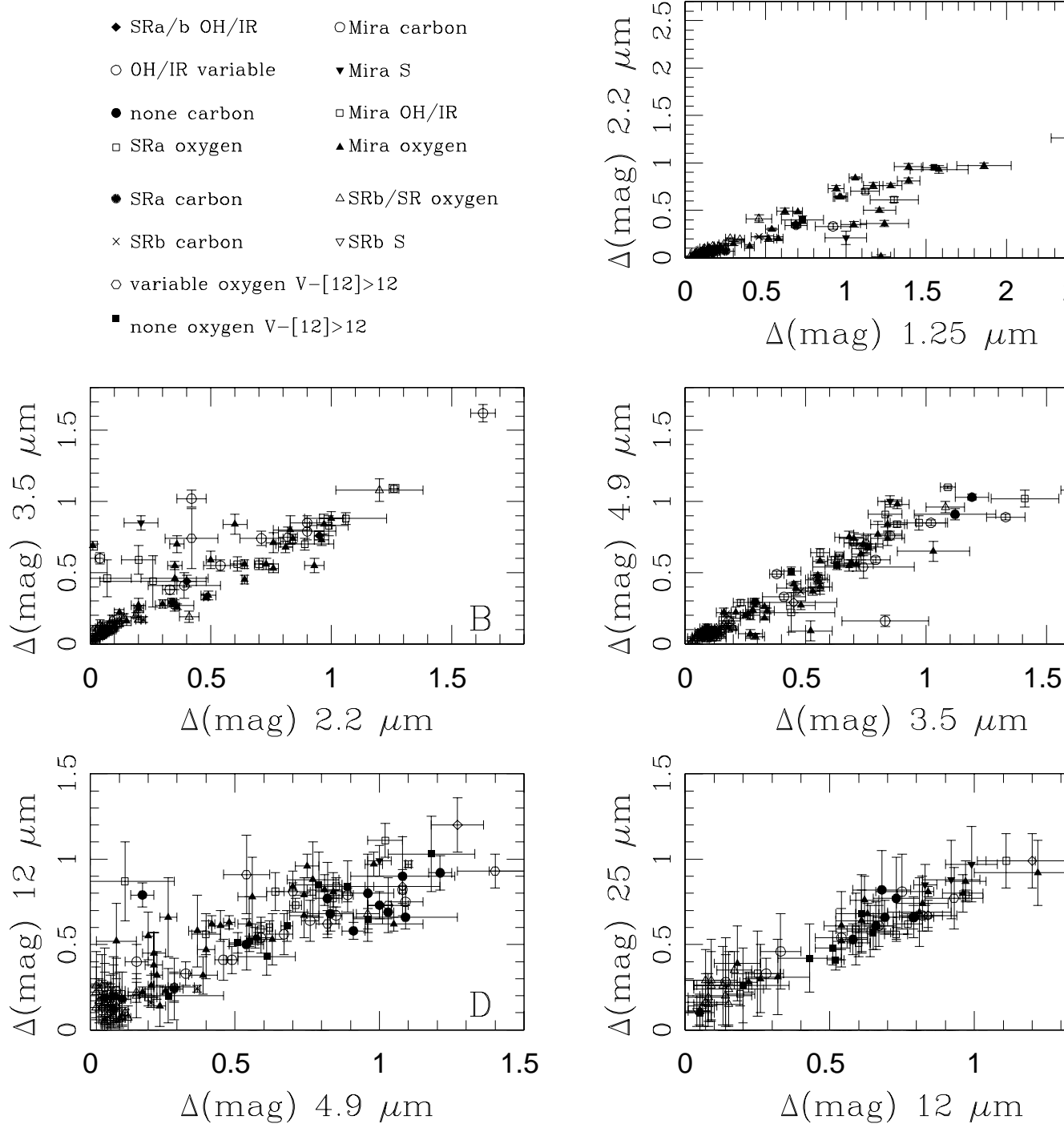


Fig. 19.— The *observed* amplitudes at the five shortest DIRBE wavelengths, plotted against those



at the next longest wavelength. Only stars with greater than  $5\sigma$  flux densities at their light curve minima are included. The symbols identified in the upper left correspond to datapoints in all five panels.

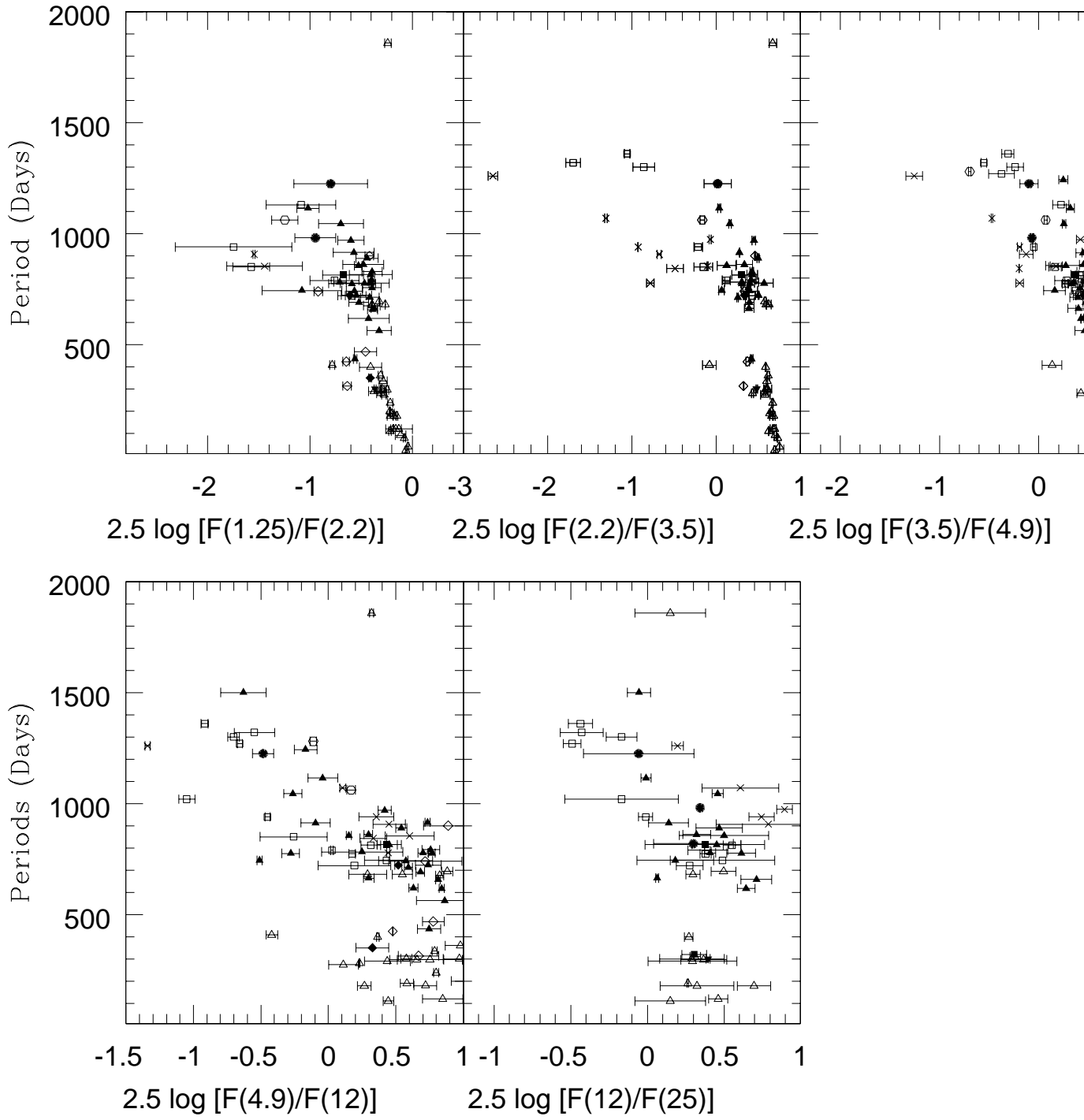


Fig. 20.— The relationship between the pulsation period and the DIRBE colors, for the 103 likely

AGB stars in the sample with known periods. The filled triangles are oxygen-rich Miras, the open squares are Miras known to contain 1662 MHz OH masers, the crosses are the carbon Miras, and the asterisks are the type S Miras. Oxygen-rich SRb stars are open triangles, carbon-rich SRA's are filled diamonds, SRA/b sources associated with OH masers are filled squares, carbon-rich SRA's are open hexagons, carbon-rich SRbs are open diamonds, and SRb's that are optical type S stars are upside down filled triangles.

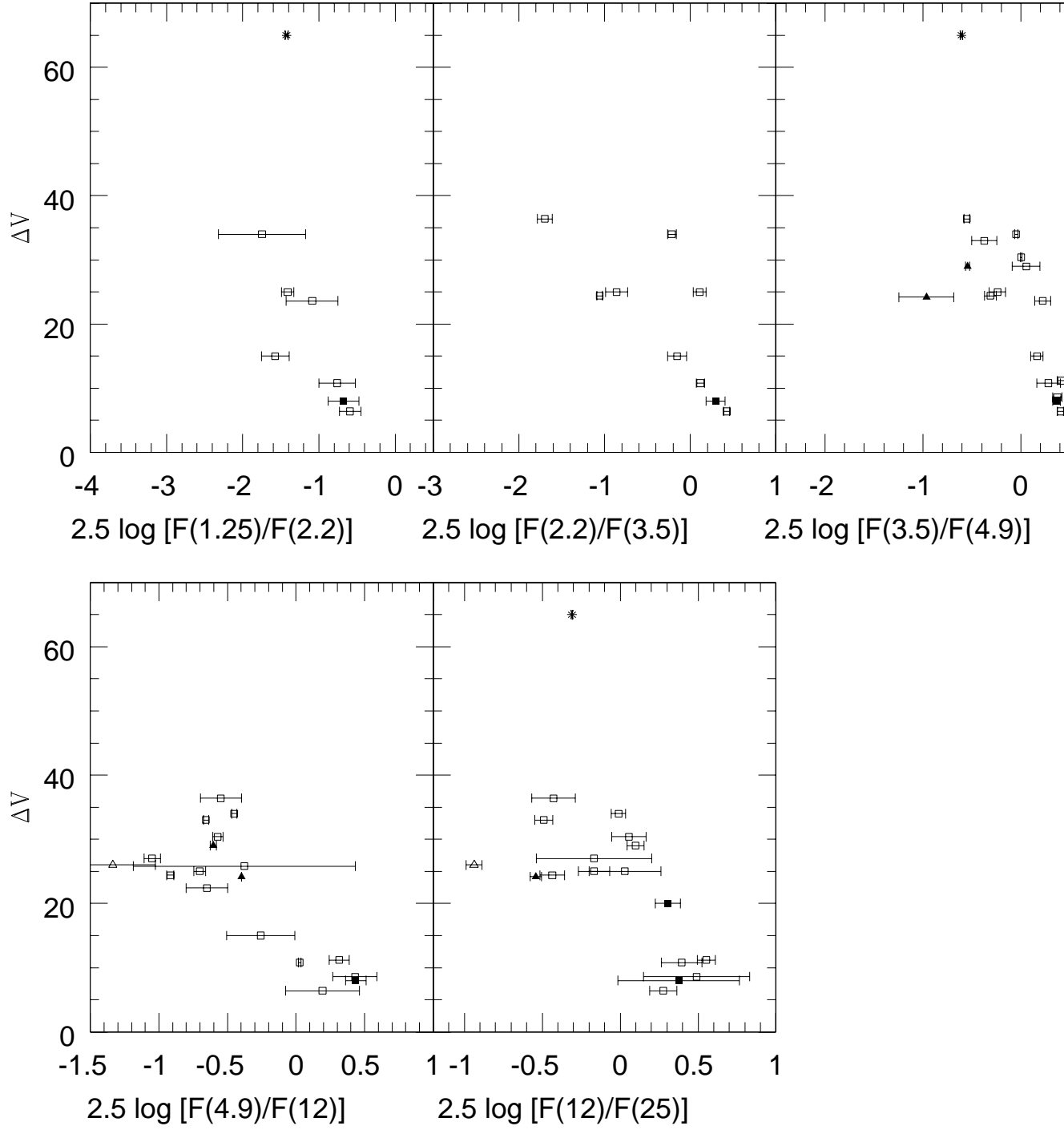


Fig. 21.— For the OH/IR stars with velocity separations  $\Delta V$  for the 1612 MHz OH line available

from Chen et al. (2001),  $\Delta V$  is plotted against the time-averaged DIRBE flux ratios for the six shortest DIRBE wavelengths. The Mira OH/IR stars are plotted as open squares and the semi-regular OH/IR stars U Men and R Crt are filled squares. The unspecified variable OH/IR stars are filled triangles, with the exception of the sole LRS type ‘A’ star in the sample, OH 338.1+6.4, which is plotted as an open triangle. VY CMa, an unspecified variable OH/IR star known to be a supergiant, is plotted as an asterisk.

Table 1. Sample

IRAS Name	Other Name	Object Type	Spectral Type	LRS Type	V mag	Period (Days)
Available in the Electronic Astronomical Journal at <a href="http://www.journals.uchicago.edu/AJ">http://www.journals.uchicago.edu/AJ</a>						

Table 2. VARIABILITY TYPES vs. OPTICAL SPECTRAL TYPES

OPTICAL TYPE	VARIABILITY TYPE														TOTAL
	Mira	SRa	SRb	SRc	SR	Lb	Lc	L	variable	Z+S	IN	R	E	none	
M	58	5	33	6	3	10	2		9	1				3	130
S	3		1												4
C	14	2	5			4			1					4	30
K	1					1			4				1	1	8
F														1	1
None	6						1		5					16	28
HII/SF												1		3	4
PN									1						1
post-AGB											1				1
<b>TOTAL</b>	82	7	39	6	3	15	2	1	20	1	1	1	1	28	207

Table 3. IRAS vs. OPTICAL SPECTRAL TYPES

OPTICAL TYPE	IRAS LRS TYPE										TOTAL
	A	C	E	F	S	H	I	P	U		
M	1	1	91	17	19		1				130
S			4								4
C		29			1						30
K				1	6					1	8
F					1						1
None		16	11							1	28
H II/SF							3		1		4
PN							1				1
post-AGB									1		1
<b>TOTAL</b>	1	46	106	18	27	4	1	2	2		207



Table 4. VARIABILITY TYPES vs. IRAS LRS SPECTRAL TYPES

LRS TYPE	VARIABILITY TYPE													TOTAL	
	Mira	SRa	SRb	SRc	SR	Lb	Lc	L	variable	Z+S	IN	R	E		none
A									1						1
C	19	2	5		1	3			3					13	46
E	51	5	20	3	2	5		1	8	1				10	106
F	11		5	1		1									18
S			8	2		6	2		6				1	2	27
H									1					3	4
I			1												1
P											1	1			2
U	1								1						2
<b>TOTAL</b>	82	7	39	6	3	15	2	1	20	1	1	1	1	28	207

Table 5. DIRBE PHOTOMETRY

IRAS	Other	1.25 $\mu\text{m}$						2.2 $\mu\text{m}$					
Name	Name	$F_\nu$	$\sigma$	$\langle\text{err}\rangle$	$\Delta\text{mag}$	$\sigma\Delta\text{mag}$	N	$F_\nu$	$\sigma$	$\langle\text{err}\rangle$	$\Delta\text{mag}$	$\sigma\Delta\text{mag}$	N
Available in the Electronic Astronomical Journal at <a href="http://www.journals.uchicago.edu/AJ">http://www.journals.uchicago.edu/AJ</a>													

Table 6. MEAN DIRBE COLORS

Variability Type	Spectral Type	V-[12] Limit	Lum Class	2.5 LOG F <sub>1.25</sub> /F <sub>2.2</sub>		2.5 LOG F <sub>2.2</sub> /F <sub>3.5</sub>		2.5 LOG F <sub>3.5</sub> /F <sub>4.9</sub>		2.5 LOG F <sub>4.9</sub> /F <sub>12</sub>		2.5 LOG F <sub>12</sub> /F <sub>25</sub>	
Mira	OH/IR			-1.19 ± 0.46	9	-0.38 ± 0.68	9	0.06 ± 0.31	15	-0.33 ± 0.45	16	0.04 ± 0.35	14
Mira	oxygen			-0.59 ± 0.28	27	0.26 ± 0.29	25	0.38 ± 0.19	33	0.15 ± 0.70	33	0.24 ± 0.31	20
Mira	carbon			-1.50 ± 0.07	2	-0.87 ± 0.77	9	-0.53 ± 0.56	14	-0.14 ± 0.70	12	0.46 ± 0.27	12
Mira	S			-0.87 ± 0.11	2	0.02	1	-0.08 ± 0.02	2	-0.48	1	0.20 ± 0.22	3
SRa/b	OH/IR			-0.90 ± 0.32	2	0.12 ± 0.24	2	0.24 ± 0.17	2	-0.06 ± 0.70	2	0.19 ± 0.27	3
SRa	oxygen			-0.51 ± 0.14	2	0.34	1	0.60 ± 0.20	2	0.42 ± 0.14	2		0
SRa	oxygen		I/II		0		0	0.60	1	0.74	1	0.52	1
SRa	carbon			-1.25	1	-0.17	1	-0.31 ± 0.54	2	0.03 ± 0.20	2		0
SR/SRb	oxygen		I/II	-0.25 ± 0.14	31	0.56 ± 0.30	29	0.71 ± 0.23	32	0.73 ± 0.43	33	0.33 ± 0.14	14
SRb	oxygen			-0.08	1		0		0		0		0
SRb	carbon			-0.62 ± 0.20	5	0.37 ± 0.06	4	0.89 ± 0.20	5	0.71 ± 0.15	5		0
SRb	S			-0.36	1	0.48	1	0.87	1		0	0.40	1
SRc	oxygen			-0.15 ± 0.11	6	0.64 ± 0.04	6	0.80 ± 0.10	4	0.64 ± 0.34	4	0.28 ± 0.11	2
L/Lb	oxygen			-0.22 ± 0.31	8	0.62 ± 0.15	9	0.76 ± 0.17	11	0.81 ± 0.70	9	0.61 ± 0.49	3
Lb	carbon			-0.58 ± 0.02	2	0.38	1	0.61 ± 0.94	3	0.94 ± 0.35	3		0
Lc	oxygen			-0.07	1	0.72	1	0.92	1	1.40	1	0.89 ± 0.06	2
Variable	OH/IR				0		0	-0.75 ± 0.30	2	-0.78 ± 0.49	3	-0.74 ± 0.28	2
Variable	OH/IR		I/II		0		0		0		0		0
Variable	oxygen	<5		0.14 ± 0.11	5	0.76 ± 0.02	5	0.87 ± 0.03	5	1.51 ± 0.04	5	1.02	1
Variable	oxygen	>12		-0.56 ± 0.52	2	0.36 ± 0.25	3	0.56 ± 0.27	4	-0.09 ± 0.34	5	0.33	1
Variable	oxygen		I/II		0		0		0		0	0.40	1
Variable	carbon				0		0	-0.63	1	-0.26 ± 0.86	3	0.37 ± 0.45	2
None	oxygen	<5		0.14 ± 0.01	2	0.72 ± 0.04	2	0.95 ± 0.07	2	1.44 ± 0.09	2		0
None	oxygen	>12			0		0	-0.14 ± 0.12	2	-0.61 ± 0.30	10	-0.07 ± 0.14	7
None	oxygen		I/II	0.83	1	0.84	1	0.65	1	1.75	1		0
None	carbon				0		0	-0.89 ± 0.26	3	-0.27 ± 0.55	10	0.33 ± 0.16	7

Table 7. MEAN DIRBE AMPLITUDES OF VARIATION

Var Type	Spectral Type	V-[12] Limit	Lum Class	1.25 $\mu\text{m}$			2.2 $\mu\text{m}$			3.5 $\mu\text{m}$			4.9 $\mu\text{m}$		
				$\langle\Delta\text{mag}\rangle$	$\langle\sigma\rangle$	N	$\langle\Delta\text{mag}\rangle$	$\langle\sigma\rangle$	N	$\langle\Delta\text{mag}\rangle$	$\langle\sigma\rangle$	N	$\langle\Delta\text{mag}\rangle$	$\langle\sigma\rangle$	N
Mira	OH/IR			1.46± 0.65	0.10	4	0.60± 0.38	0.10	12	0.68± 0.31	0.07	15	0.62± 0.30	0.06	16
Mira	oxygen			0.90± 0.44	0.07	26	0.53± 0.30	0.03	27	0.53± 0.23	0.05	33	0.47± 0.27	0.04	34
Mira	carbon			0.92	0.11	1	0.67± 0.44	0.07	10	0.81± 0.37	0.07	12	0.74± 0.36	0.05	13
Mira	S			1.19± 0.27	0.15	2	0.21	0.07	1	0.99± 0.20	0.05	2	1.00	0.04	1
SRa/b	OH/IR			0.80± 0.72	0.08	3	0.68± 0.39	0.03	2	0.43± 0.34	0.03	3	0.59± 0.12	0.03	2
SRa	oxygen			0.36± 0.45	0.04	2	0.50	0.01	1	0.21± 0.19	0.04	2	0.11± 0.10	0.05	2
SRa	oxygen		I/II		0.04	0		0.01	0	0.30	0.15	1	0.09	0.01	1
SRa	carbon			0.46	0.05	1	0.22	0.01	1	0.33± 0.22	0.03	2	0.29± 0.11	0.01	2
SRb	oxygen			0.15± 0.09	0.03	29	0.12± 0.21	0.02	31	0.14± 0.18	0.03	33	0.10± 0.16	0.02	33
SRb	oxygen		I/II	0.03	0.02	1	0.01	0.01	1	0.05	0.02	1	0.02	0.02	0
SRb	carbon			0.28± 0.24	0.05	5	0.11± 0.13	0.02	5	0.13± 0.09	0.03	5	0.12± 0.10	0.03	5
SRb	S			0.10	0.03	1	0.01	0.01	1	0.04	0.02	1	0.03	0.03	0
SRc	oxygen			0.09± 0.04	0.03	6	0.06± 0.02	0.01	6	0.07± 0.03	0.03	6	0.06± 0.02	0.02	4
Lb	oxygen			0.08± 0.06	0.03	8	0.09± 0.13	0.02	9	0.10± 0.09	0.04	11	0.07± 0.08	0.03	11
Lb	carbon			0.15± 0.05	0.09	2	0.10	0.02	1	0.09± 0.02	0.06	2	0.12± 0.13	0.04	4
Lc	oxygen			0.05± 0.01	0.03	2	0.02	0.01	1	0.04± 0.00	0.02	2	0.02	0.01	1
variable	OH/IR				0.03	0		0.01	0	0.45	0.18	1	0.88± 0.52	0.10	3
variable	OH/IR		I/II		0.03	0		0.01	0	0.16	0.02	1	0.10	0.10	0
variable	oxygen	<5		0.04± 0.01	0.03	6	0.01± 0.00	0.01	5	0.03± 0.01	0.02	6	0.01± 0.00	0.02	5
variable	oxygen	>12		0.12± 0.04	0.04	2	0.51± 0.35	0.06	4	0.43± 0.37	0.09	4	0.39± 0.30	0.06	5
variable	oxygen		I/II		0.04	0		0.06	0	0.09	0	0	0.06	0.06	0
variable	carbon				0.04	0		0.06	0	0.09	0	0	1.08± 0.29	0.08	3
none	oxygen	<5		0.04± 0.01	0.03	2	0.01± 0.01	0.01	2	0.02± 0.00	0.03	2	0.03± 0.01	0.02	2
none	oxygen	>12			0.03	0		0.01	0	0.63	0.05	1	0.72± 0.28	0.11	9
none	oxygen		I/II	0.03	0.03	1	0.01	0.01	1	0.03	0.03	1	0.02	0.02	1
none	carbon				0.03	0		0.01	0	1.16± 0.05	0.12	2	0.87± 0.27	0.07	13

Table 8. MEAN AMPLITUDE RATIOS

Variability Type	Spectral Type	V-[12] Limit	Lum Class	1.25/2.2 $\Delta\text{mag}/\Delta\text{mag}$	N	2.2/3.5 $\Delta\text{mag}/\Delta\text{mag}$	N	3.5/4.9 $\Delta\text{mag}/\Delta\text{mag}$	N	4.9/12 $\Delta\text{mag}/\Delta\text{mag}$	N	12/25 $\Delta\text{mag}/\Delta\text{mag}$	N
Mira	OH/IR			$1.88 \pm 0.27$	3	$1.19 \pm 0.07$	6	$1.08 \pm 0.20$	12	$0.99 \pm 0.11$	8	$1.22 \pm 0.06$	6
Mira	oxygen			$1.99 \pm 0.69$	21	$1.09 \pm 0.32$	24	$1.20 \pm 0.26$	28	$0.98 \pm 0.25$	15	$1.02 \pm 0.14$	6
Mira	carbon			2.79	1	$0.92 \pm 0.24$	7	$1.22 \pm 0.24$	8	$1.28 \pm 0.18$	8	$1.17 \pm 0.07$	3
Mira	S				0		0	0.85	1	1.01	1	0.98	1
SRa/b	OH/IR			$1.73 \pm 0.14$	2	$1.08 \pm 0.24$	2	$0.99 \pm 0.18$	2	$1.06 \pm 0.08$	2		0
SRa	oxygen			1.36	1	1.47	1	1.89	1	1.12	1		0
SRa	oxygen		I/II		0		0		0		0		0
SRa	carbon			2.09	1	1.29	1	$1.05 \pm 0.34$	2	$1.43 \pm 0.16$	2		0
SRb	oxygen			$1.89 \pm 0.73$	11	$0.84 \pm 0.21$	10	$1.45 \pm 0.34$	9	$1.39 \pm 0.26$	2		0
SRb	oxygen		I/II		0		0		0		0		0
SRb	carbon			$2.71 \pm 0.97$	2	1.17	1	1.00	1		0		0
SRb	S				0		0		0		0		0
SRc	oxygen				0		0		0	0.90	1		0
Lb	oxygen			$1.65 \pm 0.33$	2		0		0		0		0
Lb	carbon				0		0		0		0		0
Lc	oxygen				0		0		0		0		0
var	OH/IR				0		0		0	$1.17 \pm 0.16$	2	$1.23 \pm 0.03$	2
var	OH/IR		I/II		0		0		0		0		0
var	oxygen	<5			0		0		0		0		0
var	oxygen	>12			0	1.09	1	1.07	1	0.86	1		0
var	oxygen		I/II		0		0		0		0		0
var	carbon				0		0		0	$1.41 \pm 0.13$	2		0
none	oxygen	<5			0		0		0		0		0
none	oxygen	>12			0		0	1.15	1	$1.20 \pm 0.24$	3	$1.20 \pm 0.09$	2
none	oxygen		I/II		0		0		0		0		0
none	carbon				0		0	$1.19 \pm 0.05$	2	$1.44 \pm 0.16$	6	$1.11 \pm 0.08$	3

This figure "bsmith\_fig3.gif" is available in "gif" format from:

<http://arxiv.org/ps/astro-ph/0305067v2>

This figure "bsmith\_fig4.gif" is available in "gif" format from:

<http://arxiv.org/ps/astro-ph/0305067v2>